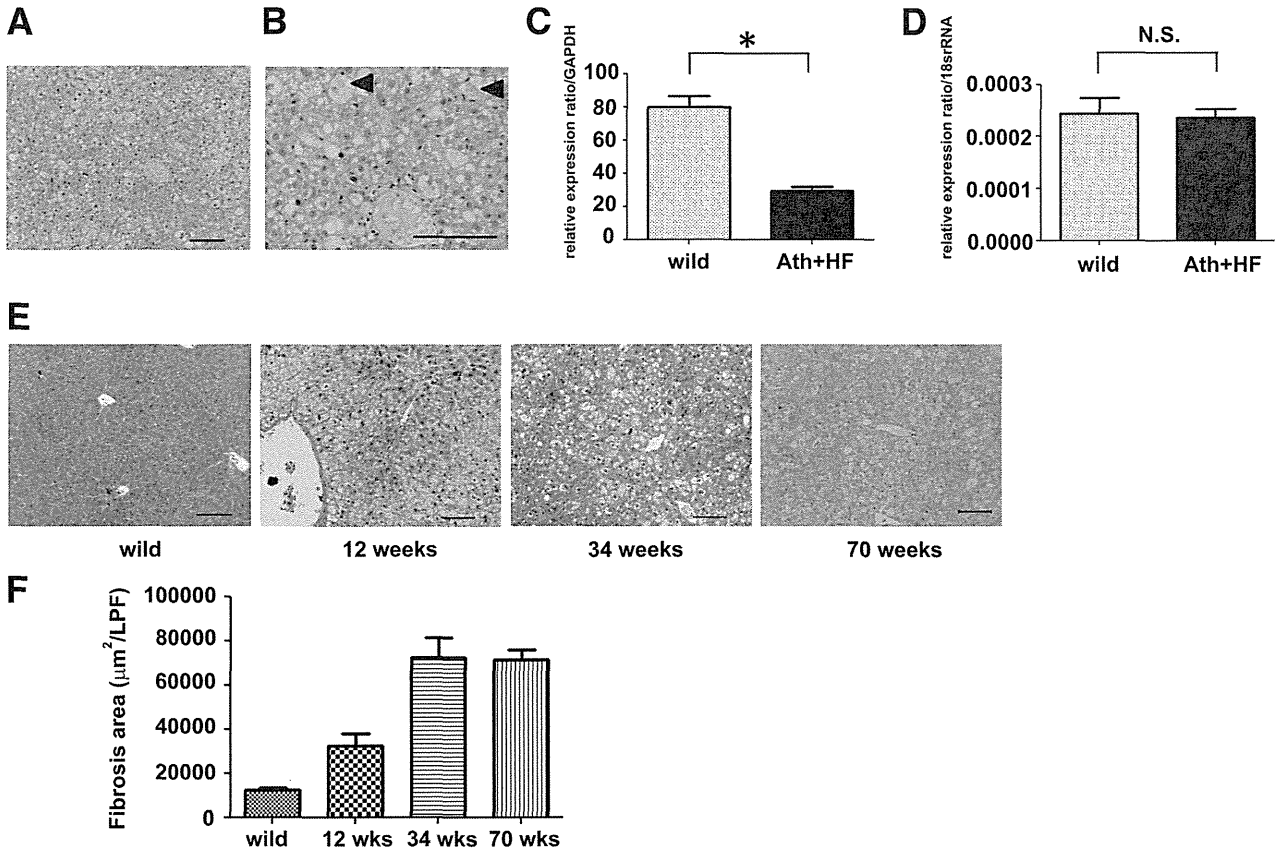

Fig. 1. Characteristics of the steatohepatitis murine model. Eight-week-old C57Bl/6 female mice were fed an Ath+HF diet. Liver tissue was obtained after 34 weeks, sectioned, and histologically examined with hematoxylin and eosin staining in (A,B) mice fed an Ath+HF diet for 34 weeks. Arrowheads indicate a Mallory-Denk body in a hepatocyte with ballooning. Parenchymal cells were isolated from 32-week-old C57Bl/6 wild-type female mice or Ath+HF mice that started the diet at 8 weeks old and continued for 24 weeks. Expression of (C) albumin and (D) AFP was assessed by reverse-transcription polymerase chain reaction (RT-PCR), n = 4, $*P < 0.05$. (E) Fibrosis was histologically examined with Azan staining in liver tissue of mice fed the Ath+HF diet for 12, 34, and 70 weeks. (F) Fibrosis areas of mice at 12, 34, and 70 weeks per ×100 low-power field were calculated for five visual fields. Bars: standard error. Scale bars = 100 μm.

in mice fed an Ath+HF diet for 32 or 36 weeks, respectively. Two weeks after the last injection the mice were euthanized and the therapeutic effects were assessed. The expression of albumin (Fig. 4A) was restored in hepatic parenchymal cells of cirrhotic mice at 2 weeks after the last injection, suggesting that ADSC treatment restored parenchymal cell function. The expression of AFP was also increased by ADSC treatment (Fig. 4B), implying enhanced regeneration of hepatic parenchymal cells. Similar effects were observed with a reduced number of (2×10^4) GFP-ADSCs (Supporting Fig. 2A,B).

We also assessed the effect of ADSC injection on fibrosis in cirrhotic mice. Liver tissue stained with Azan and anticollagen type IV antibody showed that ADSC administration reduced fibrosis compared to control animals (Fig. 5A,B; Supporting Fig. S3A,B). We also evaluated immunohistochemical staining of α-SMA, a marker of stellate cells, which are largely responsible for developing fibrosis. These results demonstrated that the number of α-SMA$^+$ cells was reduced by ADSC treatment (Fig. 5C-E), suggesting that ADSCs suppress the activity of stellate cells and ameliorate liver fibrosis.

Gene Expression Profiling of Cirrhotic Livers Following ADSC Treatment. We examined the gene expression profile of the livers in the NASH mouse model of cirrhosis by DNA microarray to determine whether administration of ADSCs was therapeutically beneficial. We identified expression of 1,249 gene probes that were significantly affected by ADSC injection. Clustering analysis of gene expression using these gene probes distinguished between ADSCs-treated mice and PBS-treated mice (Fig. 6A). Among 1,249 genes, 797 were up-regulated and 452 were down-regulated by ADSC treatment. Regarding matrix metalloproteinase (MMP), expressions of MMP-8 and MMP-9 were enhanced in the liver of NASH mice treated with PBS compared to the wild type; this enhancement was removed by ADSC treatment

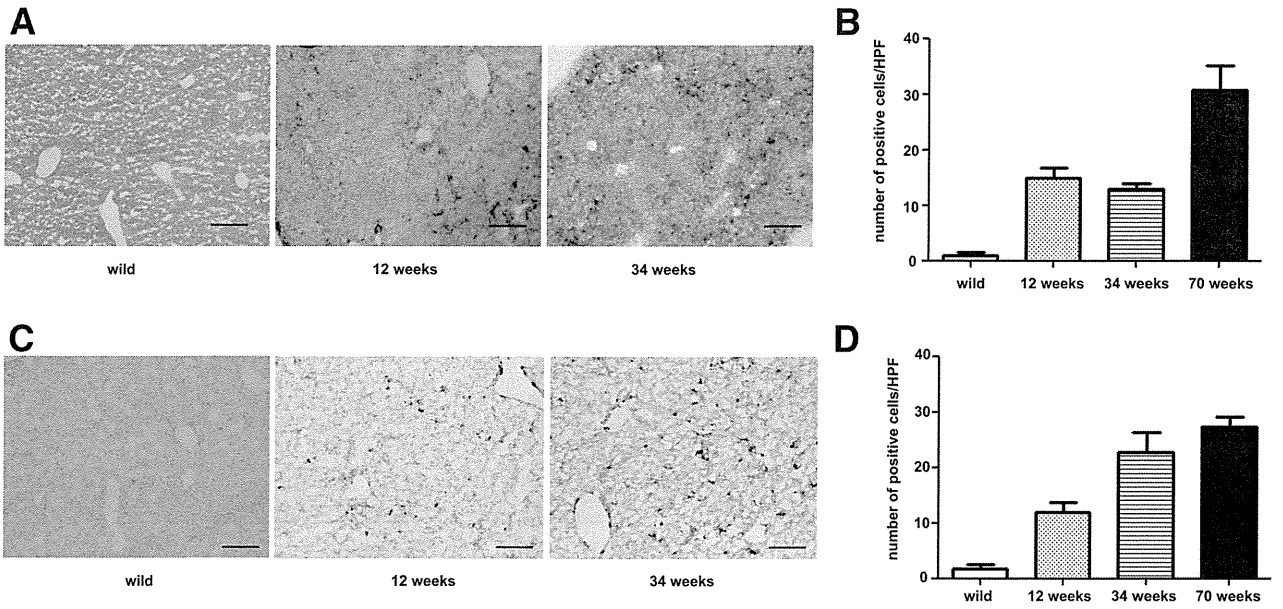

Fig. 2. Immunohistochemical staining of a steatohepatitis liver. Eight-week-old female C57Bl/6 female mice were fed an Ath+HF diet. Liver tissue was obtained from these mice or from wild-type animals after 12, 34, and 70 weeks. Immunohistochemical staining was performed for (A) Gr-1$^+$ or (C) CD11b$^+$ cells and the number of positive cells in a high-power field was counted for five visual fields for (B) Gr-1 or (D) CD11b at each timepoint.

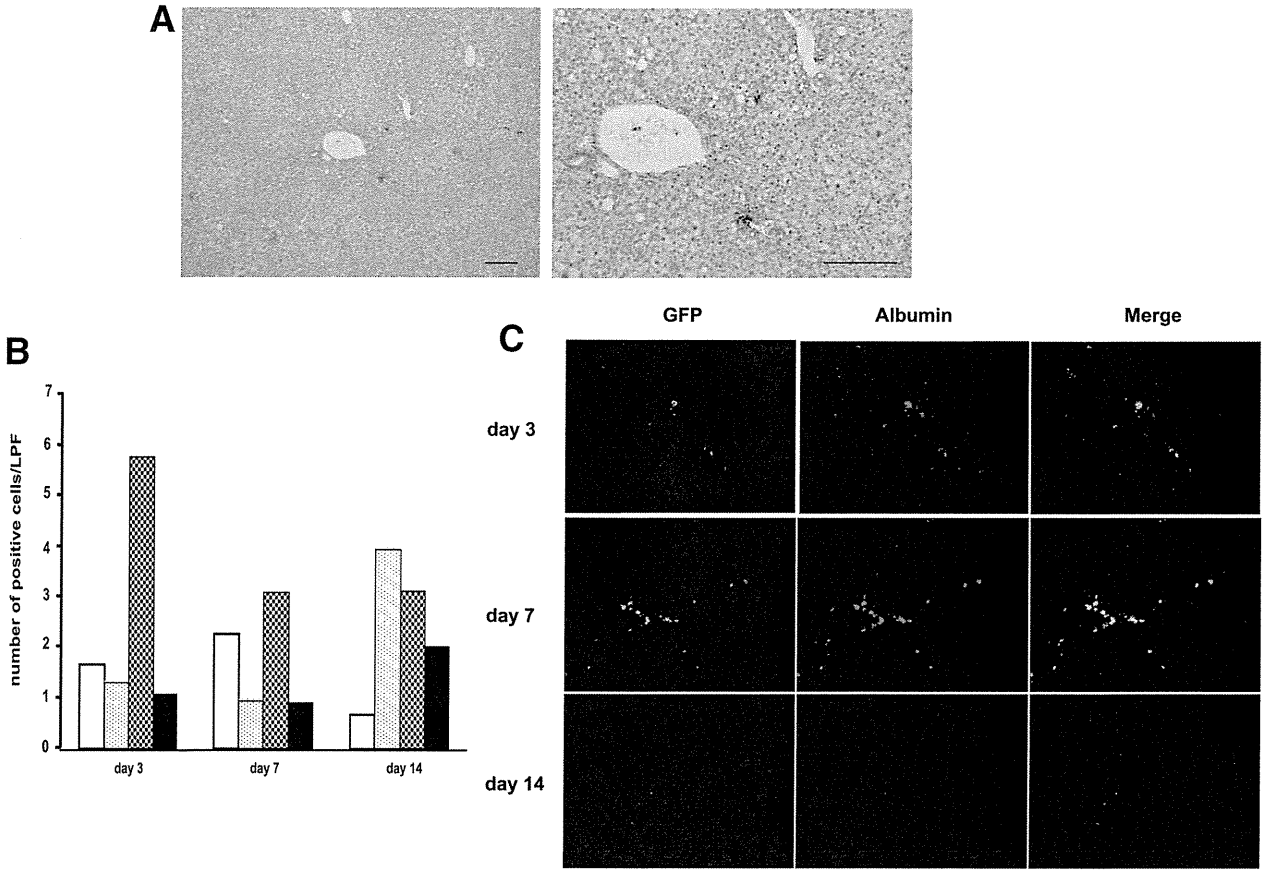

Fig. 3. Distribution of ADSCs and albumin expression in the livers of steatohepatitis mice. ADSCs from GFP-Tg mice (1×10^5) were injected into the splenic subcapsule of cirrhotic C57Bl/6 mice fed the Ath+HF diet for 32 weeks. After 3, 7, and 14 days, liver tissue was obtained and examined by immunohistochemical staining for (A) GFP; Scale bars = 100 μm. (B) GFP$^+$ cells in the liver were counted per ×100 low-power field and five visual fields were calculated. White bar, caudate lobe; dotted bar, left lobe; hatched bar, middle lobe; black bar, right lobe. (C) Immunohistochemical staining for GFP or albumin antibody. Magnification, ×100.

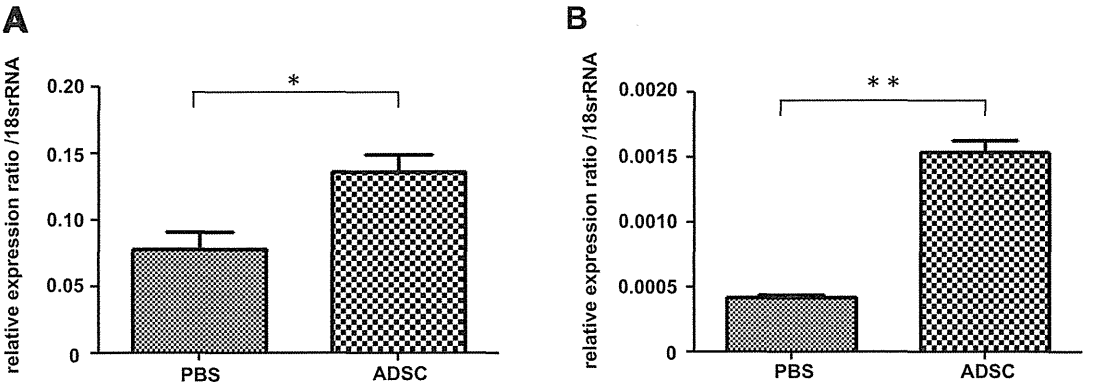

Fig. 4. Albumin and AFP expression in hepatic parenchymal cells. ADSCs from GFP-Tg mice (1×10^5) were injected twice every 2 weeks into the splenic subcapsule of cirrhotic C57Bl/6 mice fed an Ath+HF diet for 32 weeks. Control mice received PBS injections. Two weeks after the last injection, liver tissue was obtained and parenchymal cells were isolated for real-time PCR. Expressions of (A) albumin and (B) AFP were normalized relative to that of 18S ribosomal RNA (rRNA); $*P < 0.05$, $**P < 0.01$.

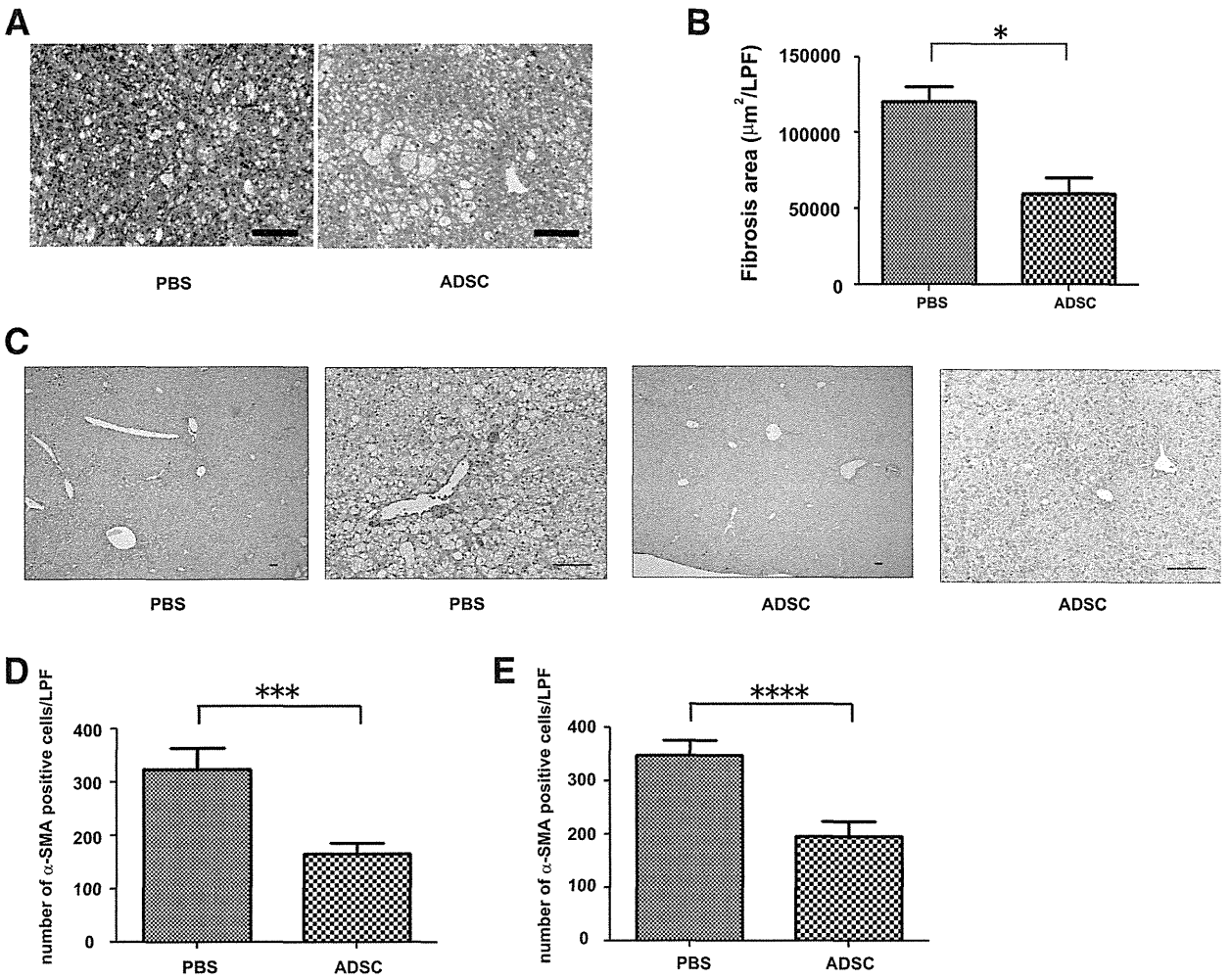

Fig. 5. Effect of ADSCs on liver fibrosis. ADSCs from GFP-Tg mice (1×10^5) were injected twice every 2 weeks into the splenic subcapsule of cirrhotic C57Bl/6 mice fed the Ath+HF diet for 32 weeks. Control mice received PBS injections. (A) Two weeks after the last injection, liver tissue was obtained, sectioned, and histologically examined with hematoxylin and eosin staining. (B) Fibrosis was examined by Azan staining and fibrotic area was quantified by image-analysis. (C) Immunohistochemical staining of liver sections for α-SMA. Scale bars = 100 μm. (D,E) The number of α-SMA+ cells in liver tissues obtained 1 (D) or 2 weeks (E) after the last ADSC injection determined by microscopy of five low-power fields (×100); $***P < 0.005$, $****P = 0.0001$.

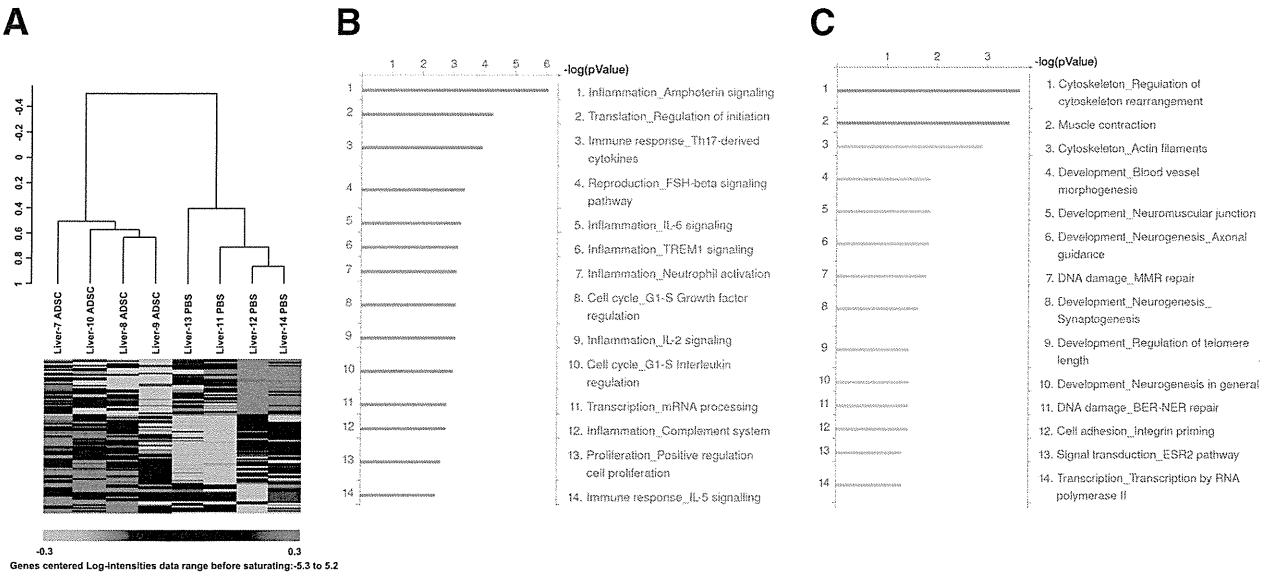

Fig. 6. Hepatic gene expression analysis. ADSCs from GFP-Tg mice (1×10^5) were injected twice every 2 weeks into the splenic subcapsule of cirrhotic C57Bl/6 mice fed an Ath+HF diet for 40 weeks. Control mice received PBS injections. Two weeks later, liver tissue was subjected to RNA isolation and gene expression using DNA microarrays. (A) Unsupervised clustering analysis was performed using probes for 1,249 genes whose expression differed significantly between the PBS and ADSC groups. (B) The biological processes of 452 genes whose expression was down-regulated in the ADSCs group compared to the PBS group were analyzed. (C) The biological processes of 797 genes whose expression was up-regulated in the ADSCs group compared to the PBS group were analyzed.

(Supporting Fig. S4). Biological process analysis indicated that the down-regulated genes were primarily related to inflammation and the immune response (Fig. 6B), and the up-regulated genes were related to tissue construction and development (Fig. 6C). Thus, gene expression analysis of liver tissue demonstrated that ADSCs treatment caused anti-inflammatory effects, as well as regeneration/repair effects, in the livers of a NASH mouse model of cirrhosis.

Anti-inflammatory Effects of ADSC Treatment. The fundamental underlying pathophysiology of steatohepatitis-induced cirrhosis is persistent hepatic inflammation caused by steatosis in hepatocytes.[16] We examined how ADSCs affected persistent inflammation of the liver in NASH mice at 2 weeks after the last injection of ADSCs. Immunohistochemical staining showed that the number of $CD11b^+$ cells accumulating in the livers of cirrhotic mice decreased with ADSC treatment compared to those of PBS-treated mice (Fig. 7A). The number of $Gr\text{-}1^+$ cells in cirrhotic liver also decreased with ADSC treatment (Fig. 7A), suggesting that ADSCs affect granulocytes and antigen-presenting cell lineage.

We further examined whether ADSC treatment affected the lymphocyte lineage of T cells, since they also play an important role in immune regulation of steatohepatitis.[17] We isolated lymphocytes from the livers of mice treated with ADSCs and examined the $CD4^+$ and $CD8^+$ T cells using flow cytometry. $CD8^+$ T cells were found predominantly in cirrhotic mice treated with PBS (Fig. 7B,C). However, when the mice were treated with ADSCs the number of $CD4^+$ T cells increased and was comparable to that of $CD8^+$ T cells, indicating that ADSC treatment affected T-cell subpopulations.

Gene Expression Profiling of Hepatic Inflammatory Cells Following ADSC Treatment. We further examined how injected ADSCs affected hepatic inflammatory cell gene expression by using DNA microarrays. By filtering the results from 5,065 gene probes, completely discernible clusters of gene expression were formed between ADSC- and PBS-treated animals (Fig. 8A). We identified the expression of 873 genes that were significantly up-regulated at least 2-fold with ADSC injection and 658 genes that were down-regulated. Most of the chemokines and cytokines whose expression was significantly affected by ADSCs were down-regulated (Supporting Table S1). Using the publicly available gene expression database for hematopoietic cells (GSE27787) and various types of helper T cells (GSE14308), we examined features of these affected genes in the context of immunomodulatory cells. Among the hematopoietic cells, genes with available symbol annotation were predominately $Gr\text{-}1^+$ and $CD11b^+$ cells from granulocyte and macrophage lineages (Fig. 8B). Among helper T-cell populations,

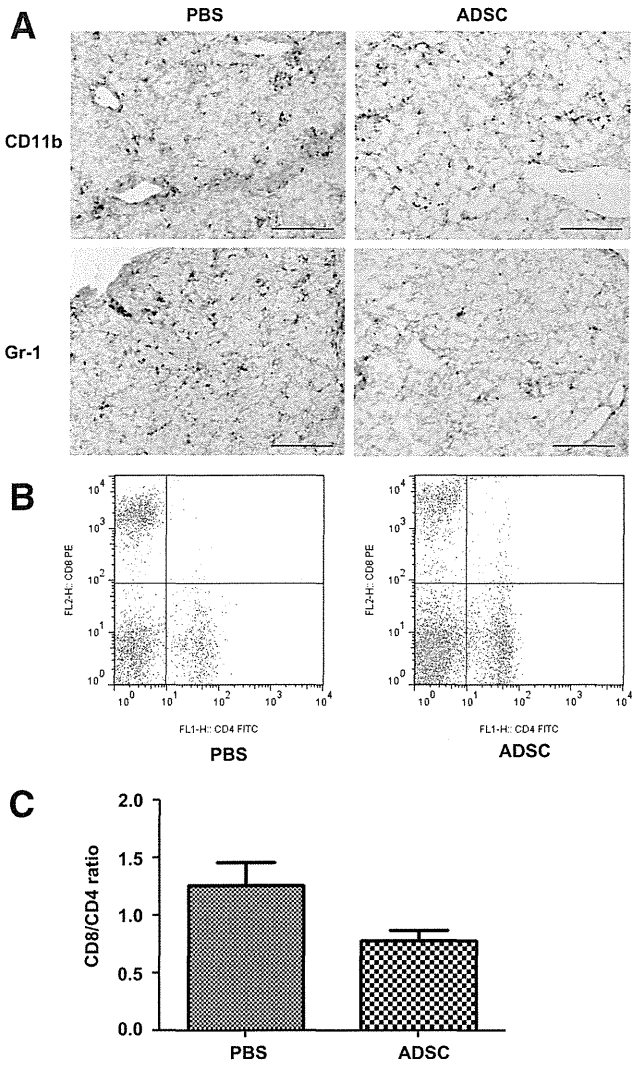

Fig. 7. Effect of ADSCs on inflammatory cells in the cirrhotic liver. ADSCs from GFP-Tg mice (1×10^5) were injected twice every 2 weeks into the splenic subcapsule of cirrhotic C57Bl/6 mice fed the Ath+HF diet for 32 weeks. Control mice received PBS injections. Two weeks later, liver tissue was obtained and immunohistochemical staining of (A) $CD11b^+$ and (B) $Gr\text{-}1^+$ cells was performed. Inflammatory cells in the liver were also isolated and stained with FITC-labeled anti-CD4 and PE-labeled CD8 antibodies. (C) The ratio of $CD8^+$ cells to $CD4^+$ cells was calculated. N = 4 ± standard error.

annotated genes included activated Th1, Th2, and Th17 cell types (Fig. 8C). We also isolated $CD4^+$T cells from hepatic inflammatory cells obtained from NASH mice fed an Ath+HF diet for 12 weeks, then treated with ADSC. Expressions of the Th1, Th2, and Th17 cytokines, interferon-γ, interleukin (IL)−4, IL-10, and IL-17, the Th17-related cytokine transforming growth factor beta (TGF-β), and Foxp3, a representative transcription factor of regulatory T cells, were down-regulated by ADSC treatment (Supporting Fig. S5).

These results suggest that ADSC treatment suppresses inflammation in the NASH mouse model primarily by down-regulating granulocytes, antigen-presenting cells, and activated helper T cells.

Discussion

This study investigated the therapeutic effect of ADSCs in a NASH murine model of cirrhosis. This model is relevant to clinical NASH, with similar pathological features established by an atherogenic high-fat diet, including the appearance of steatosis, ballooning, and Mallory-Denk bodies in hepatocytes, infiltration of inflammatory cells, and pericellular fibrosis. Our results demonstrate that ADSC injection is therapeutically beneficial for cirrhosis in this murine model through restoration of albumin expression in hepatic parenchymal cells, amelioration of fibrosis, and suppression of persistent hepatic inflammation.

Gene expression analysis of the liver in this cirrhotic mouse model revealed that ADSC injection affects biological processes relating to anti-inflammatory and regeneration/repair pathways. The anti-inflammatory effects are mediated by ADSC targeting of $Gr\text{-}1^+$, $CD11b^+$, and helper T-cell lineages. In patients with clinical NASH, the ratio of neutrophils to lymphocytes increases,[18] suggesting that granulocytes are involved in the pathogenesis of NASH. The NASH murine model used in this study produced an increased $CD8^+/CD4^+$ T-cell ratio, which is also comparable to clinical NASH patient pathology.[19] Gene expression analysis of liver tissue and hepatic inflammatory cells from NASH mice showed that Th1-, Th2-, and Th17-related genes were down-regulated by ADSC treatment. Helper T-cell activation skewed to produce Th1 cytokines is pathogenic in steatohepatitis.[20,21] In particular, Th17 is emerging as an important source of IL-17 family cytokines[22] and is involved in the hepatic inflammation in NASH.[23] Helper T cells producing Th2 cytokines such as IL-4, 5, and 13 contribute to fibrosis.[24] We conclude that activated T helper cells are responsible for the pathogenesis of steatohepatitis in the NASH murine model used in this study and that ADSCs suppress pathogenic helper T-cell activation. However, the suppression of miscellaneous effector and regulatory helper T cells by ADSCs should be further evaluated with regard to prevention of hepatocellular carcinoma, a frequent sequela to cirrhosis, since Th1 promotes antitumor immunity and Th2 down-regulates antitumor immunity.

We also observed that ADSC treatment ameliorated fibrosis and decreased the number of α-SMA^+ stellate

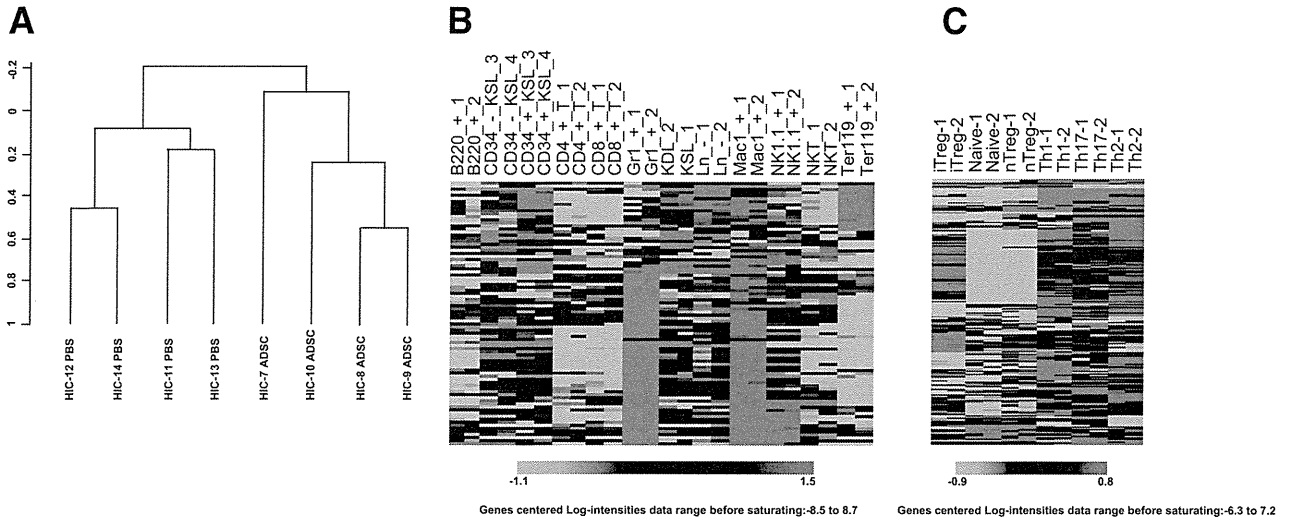

Fig. 8. Gene-expression analysis of intrahepatic inflammatory cells. ADSCs from GFP-Tg mice (1×10^5) were injected twice every 2 weeks into the splenic subcapsule of cirrhotic C57Bl/6 mice fed an Ath+HF diet for 40 weeks. Control mice received PBS injections. Inflammatory cells were isolated from the liver and gene expression examination was performed using DNA microarrays. (A) Unsupervised clustering analysis using the filtered 5,065 gene probes. HIC; hepatic inflammatory cells. (B) One-way clustering analysis using a publicly available database of hematopoietic cells (GSE27787) of 658 genes whose expression was down-regulated by ADSC treatment with available gene symbol annotations. (C) One-way clustering analysis using publicly available database of different helper T subsets (GSE14308) of 658 genes whose expression was down-regulated by ADSCs treatment with available gene symbol annotations.

cells in cirrhotic liver. When inflammation persists in the liver, fibrosis progresses due to these activated stellate cells, which are almost identical to myofibroblasts and produce extracellular matrix. Stellate cells are activated by miscellaneous factors including TGF-β and platelet-derived growth factor,[25] produced mostly from Kupffer cells. Helper T cells expressing Th2 cytokines are also involved in the development of fibrosis. Gene expression analysis of the cirrhotic livers indicated that ADSC treatment suppressed Th2-type helper T cells. Although details of how these molecules mediate fibrosis development have yet to be examined in the current NASH murine model, the antifibrotic effect of ADSCs is achieved in part by suppressing Th2-type helper T cells. We found that MMP-8 and MMP-9 enhancement in the NASH-cirrhotic liver was ameliorated by ADSC treatment. MMP-9 expression is related to the inflammation typical of steatohepatitis[26] and can ameliorate the hepatic fibrosis induced by carbon tetrachloride.[27] Further studies are needed to clarify the role of MMPs in the pathogenesis of cirrhosis as well as to explore novel therapies for this condition.

Pluripotent MSCs differentiate into several cell lineages and are a promising avenue for regenerative therapy of various impaired organs, including the liver. Although ADSCs were observed in cirrhotic livers at up to 2 weeks after injection and expressed albumin, the numbers of resident cells were not sufficient to supplement hepatic function. Therefore, pluripotency, as well as the anti-inflammatory and antifibrotic effects of ADSCs, are important for their regenerative/repair effects in liver cirrhosis. Rather than studying the effects of ADSCs on early-stage steatohepatitis, we treated mice with endstage cirrhosis with ADSCs to observe their therapeutic effects. Our results demonstrated that ADSCs can effectively resolve chronic fibrosis and decrease inflammation, thereby restoring hepatic function in endstage cirrhotic mice, implying the usefulness of this therapy as an alternative to liver transplantation.

In conclusion, ADSCs proved therapeutically beneficial and clinically relevant in regenerative therapy of a murine steatohepatitis-cirrhosis model. Clinical application of ADSCs in the treatment of cirrhosis is expected to provide a novel alternative regenerative/repair therapy for patients with cirrhosis.

References

1. D'Amico G, Garcia-Tsao G, Pagliaro L. Natural history and prognostic indicators of survival in cirrhosis: a systematic review of 118 studies. J Hepatol 2006;44:217-231.
2. Llovet JM, Burroughs A, Bruix J. Hepatocellular carcinoma. Lancet 2003;362:1907-1917.
3. Fattovich G, Stroffolini T, Zagni I, Donato F. Hepatocellular carcinoma in cirrhosis: incidence and risk factors. Gastroenterology 2004;127:S35-50.
4. Kamath PS, Kim WR. The model for end-stage liver disease (MELD). HEPATOLOGY 2007;45:797-805.
5. Stravitz RT, Carl DE, Biskobing DM. Medical management of the liver transplant recipient. Clin Liver Dis 2011;15:821-843.

6. Forner A, Llovet JM, Bruix J. Hepatocellular carcinoma. Lancet 2012;379:1245-1255.
7. Chamberlain G, Fox J, Ashton B, Middleton J. Concise review: mesenchymal stem cells: their phenotype, differentiation capacity, immunological features, and potential for homing. Stem Cells 2007;25:2739-2749.
8. Franco Lambert AP, Fraga Zandonai A, Bonatto D, Cantarelli Machado D, Pegas Henriques JA. Differentiation of human adipose-derived adult stem cells into neuronal tissue: does it work? Differentiation 2009;77:221-228.
9. Banas A, Teratani T, Yamamoto Y, Tokuhara M, Takeshita F, Osaki M, et al. Rapid hepatic fate specification of adipose-derived stem cells and their therapeutic potential for liver failure. J Gastroenterol Hepatol 2009;24:70-77.
10. Banas A, Teratani T, Yamamoto Y, Tokuhara M, Takeshita F, Quinn G, et al. Adipose tissue-derived mesenchymal stem cells as a source of human hepatocytes. HEPATOLOGY 2007;46:219-228.
11. Uccelli A, Moretta L, Pistoia V. Immunoregulatory function of mesenchymal stem cells. Eur J Immunol 2006;36:2566-2573.
12. Zuk PA, Zhu M, Ashjian P, De Ugarte DA, Huang JI, Mizuno H, et al. Human adipose tissue is a source of multipotent stem cells. Mol Biol Cell 2002;13:4279-4295.
13. Matsuzawa N, Takamura T, Kurita S, Misu H, Ota T, Ando H, et al. Lipid-induced oxidative stress causes steatohepatitis in mice fed an atherogenic diet. HEPATOLOGY 2007;46:1392-1403.
14. Furuichi K, Shintani H, Sakai Y, Ochiya T, Matsushima K, Kaneko S, et al. Effects of adipose-derived mesenchymal cells on ischemia-reperfusion injury in kidney. Clin Exp Nephrol 2012;16:579-589.
15. Brunt EM. Nonalcoholic steatohepatitis: definition and pathology. Semin Liver Dis 2001;21:3-16.
16. Cohen JC, Horton JD, Hobbs HH. Human fatty liver disease: old questions and new insights. Science 2011;332:1519-1523.
17. Inzaugarat ME, Ferreyra Solari NE, Billordo LA, Abecasis R, Gadano AC, Chernavsky AC. Altered phenotype and functionality of circulating immune cells characterize adult patients with nonalcoholic steatohepatitis. J Clin Immunol 2011;31:1120-1130.
18. Alkhouri N, Morris-Stiff G, Campbell C, Lopez R, Tamimi TA, Yerian L, et al. Neutrophil to lymphocyte ratio: a new marker for predicting steatohepatitis and fibrosis in patients with nonalcoholic fatty liver disease. Liver Int 2012;32:297-302.
19. Susca M, Grassi A, Zauli D, Volta U, Lenzi M, Marchesini G, et al. Liver inflammatory cells, apoptosis, regeneration and stellate cell activation in non-alcoholic steatohepatitis. Dig Liver Dis 2001;33:768-777.
20. Olleros ML, Martin ML, Vesin D, Fotio AL, Santiago-Raber ML, Rubbia-Brandt L, et al. Fat diet and alcohol-induced steatohepatitis after LPS challenge in mice: role of bioactive TNF and Th1 type cytokines. Cytokine 2008;44:118-125.
21. Ferreyra Solari NE, Inzaugarat ME, Baz P, De Matteo E, Lezama C, Galoppo M, et al. The role of innate cells is coupled to a Th1-polarized immune response in pediatric nonalcoholic steatohepatitis. J Clin Immunol 2012;32:611-621.
22. Ouyang W, Kolls JK, Zheng Y. The biological functions of T helper 17 cell effector cytokines in inflammation. Immunity 2008;28:454-467.
23. Tang Y, Bian Z, Zhao L, Liu Y, Liang S, Wang Q, et al. Interleukin-17 exacerbates hepatic steatosis and inflammation in non-alcoholic fatty liver disease. Clin Exp Immunol 2011;166:281-290.
24. Wynn TA. Fibrotic disease and the T(H)1/T(H)2 paradigm. Nat Rev Immunol 2004;4:583-594.
25. Wu J, Zern MA. Hepatic stellate cells: a target for the treatment of liver fibrosis. J Gastroenterol 2000;35:665-672.
26. Wanninger J, Walter R, Bauer S, Eisinger K, Schaffler A, Dorn C, et al. MMP-9 activity is increased by adiponectin in primary human hepatocytes but even negatively correlates with serum adiponectin in a rodent model of non-alcoholic steatohepatitis. Exp Mol Pathol 2011;91:603-607.
27. Higashiyama R, Inagaki Y, Hong YY, Kushida M, Nakao S, Niioka M, et al. Bone marrow-derived cells express matrix metalloproteinases and contribute to regression of liver fibrosis in mice. HEPATOLOGY 2007;45:213-222.

Cancer Immunol Immunother (2013) 62:1421–1430
DOI 10.1007/s00262-013-1447-1

ORIGINAL ARTICLE

Increase in $CD14^{+}HLA\text{-}DR^{-/low}$ myeloid-derived suppressor cells in hepatocellular carcinoma patients and its impact on prognosis

Fumitaka Arihara · Eishiro Mizukoshi · Masaaki Kitahara · Yoshiko Takata · Kuniaki Arai · Tatsuya Yamashita · Yasunari Nakamoto · Shuichi Kaneko

Received: 15 February 2013 / Accepted: 29 May 2013 / Published online: 14 June 2013

Abstract Myeloid-derived suppressor cells (MDSCs) are known as key immune regulators in various human malignancies, and it is reported that $CD14^{+}HLA\text{-}DR^{-/low}$ MDSCs are increased in hepatocellular carcinoma (HCC) patients. However, the host factors that regulate the frequency and the effect on the prognosis of HCC patients are still unclear. We investigated these issues and clarified the relationships between a feature of MDSCs and host factors in HCC patients. We examined the frequency of MDSCs in 123 HCC patients, 30 chronic liver disease patients without HCC, and 13 healthy controls by flow cytometric analysis. The relationships between the clinical features and the frequency of MDSCs were analyzed. In 33 patients who received curative radiofrequency ablation (RFA) therapy, we examined the impact of MDSCs on HCC recurrence. The frequency of MDSCs in HCC patients was significantly increased. It was correlated with tumor progression, but not with the degree of liver fibrosis and inflammation. In terms of serum cytokines, the concentrations of IL-10, IL-13, and vascular endothelial growth factor were significantly correlated with the frequency of MDSCs. In HCC patients who received curative RFA therapy, the frequency of MDSCs after treatment showed various changes and was inversely correlated with recurrence-free survival time. The frequency of MDSCs is correlated with tumor progression, and this frequency after RFA is inversely correlated with the prognosis of HCC patients. Patients with a high frequency of MDSCs after RFA should be closely followed and the inhibition of MDSCs may improve the prognosis of patients.

Keywords Myeloid-derived suppressor cells · Hepatocellular carcinoma · Radiofrequency ablation · Recurrence · Cancer

Abbreviations

MDSCs	Myeloid-derived suppressor cells
HCC	Hepatocellular carcinoma
CLD	Chronic liver disease
RFA	Radiofrequency ablation
TACE	Transcatheter arterial chemoembolization
PBMC	Peripheral blood mononuclear cell
Tregs	Regulatory T cells
HLA	Human leukocyte antigen
FGF	Fibroblast growth factor
CCL	Chemokine C–C motif ligand
G-CSF	Granulocyte colony stimulating factor
GM-CSF	Granulocyte macrophage colony stimulating factor
IP	Interferon gamma-induced protein
MCP	Monocyte chemoattractant protein
MIP	Macrophage inflammatory protein
PDGF	Platelet-derived growth factor
RANTES	Regulated upon activation, normal T cell expressed and secreted
TNF	Tumor necrosis factor
VEGF	Vascular endothelial growth factor

Electronic supplementary material The online version of this article (doi:10.1007/s00262-013-1447-1) contains supplementary material, which is available to authorized users.

F. Arihara (✉) · E. Mizukoshi · M. Kitahara · Y. Takata · K. Arai · T. Yamashita · S. Kaneko
Department of Gastroenterology, Graduate School of Medicine, Kanazawa University, 13-1, Takara-machi, Kanazawa, Ishikawa 920-8641, Japan
e-mail: bnkyo78@gmail.com; arihara@m-kanazawa.jp

Y. Nakamoto
Second Department of Internal Medicine, Faculty of Medical Sciences, University of Fukui, Matsuoka, Fukui, Japan

JAK Janus kinase
STAT Signal transducer and activator of transcription

Introduction

Hepatocellular carcinoma (HCC) is one of the most common malignancies and the third leading cause of cancer mortality globally [1, 2]. Current treatment options including surgical resection, radiofrequency ablation (RFA), liver transplantation, chemotherapy, transcatheter arterial chemoembolization (TACE), and sorafenib are reported to improve survival in HCC patients [3–7]. However, despite curative treatments for HCC, tumor recurrence rates remain high and the survival of those who have advanced HCC remains unsatisfactory [3–7]. Therefore, the development of new anti-tumor treatments for HCC remains an urgent and important field of research.

To overcome the limitations of these treatments, several immunotherapies have been developed as attractive strategies for HCC. In several studies of HCC immunotherapy, effective induction of immune-mediated cells by tumor antigen-derived peptides or antigen-presenting cells showed anti-tumor effects, but the population of patients who exhibited such effects was very small [8–12].

In previous studies, it was reported that many kinds of tumor generate a number of immune-suppressive mechanisms [13–15]. Recently, myeloid-derived suppressor cells (MDSCs) have been characterized as key immune regulators in various human cancers [15–24]. They show the capacity to inhibit T cell function and promote tumor development [15, 25]. Human MDSCs are a heterogeneous population that shows $CD11b^+$, $CD33^+$, HLA-$DR^{-/low}$ and can be divided into granulocytic $CD14^-$ and monocytic $CD14^+$ subtypes [26–28]. In most recent studies, it has been reported that $CD14^+$HLA-$DR^{-/low}$ MDSCs were increased in HCC patients and the cells inhibited the function of T cells through the induction of regulatory T cells (Tregs) [24]. Tregs represent 5–10 % of $CD4^+$ T cells and can suppress the activation and proliferation of $CD4^+$ and $CD8^+$ T cells [14, 29]. It was reported that an increased frequency of circulating Tregs was associated with poor survival of HCC patients [30]. Understanding the inhibitory mechanism of MDSCs and controlling their function are very important to develop more effective immunotherapy for HCC.

In this study, we investigate the host factors that are associated with the frequency of MDSCs in HCC patients and the effect of MDSCs on the prognosis of patients and clarify the relationships between a feature of MDSCs and host factors in HCC patients.

Materials and methods

Patients and healthy controls

Blood samples were obtained from a total of 123 HCC patients, 26 chronic liver disease (CLD) patients without HCC, and 13 healthy controls. The diagnosis of HCC was histologically confirmed in 68 patients. For the remaining 55 patients, diagnosis was made by dynamic CT or MRI. Patient characteristics and disease classification are shown in Suppl. table 1. All CLD patients without HCC underwent percutaneous liver biopsy to evaluate the disease severity according to the Metavir scoring system. In 33 patients treated with curative percutaneous RFA, blood samples were obtained on the day of treatment and 2–4 weeks after treatment, and we observed recurrence of these patients with periodic imaging studies. All subjects provided written informed consent to participate in this study in accordance with the Declaration of Helsinki. This study was approved by the regional ethics committee (Medical Ethics Committee of Kanazawa University).

Cell isolation and flow cytometric analysis

Peripheral blood mononuclear cells (PBMCs) were separated as described below; heparinized venous blood was diluted in phosphate-buffered saline (PBS) and loaded on Ficoll-Histopaque (Sigma, St. Louis, Mo.) in 50 ml tubes. After centrifugation at 2,000 rpm for 20 min at room temperature, PBMCs were harvested from the interphase, resuspended in PBS, centrifuged at 1,400 rpm for 10 min, and finally resuspended in complete culture medium consisting of RPMI (GibcoBRL, Grand Island, NY), 10 % heat inactivated FCS (Gibco BRL), 100 U/ml penicillin, and 100 μg/ml streptomycin (Gibco BRL). PBMCs were resuspended in RPMI 1,640 medium containing 80 % FCS and 10 % dimethyl sulfoxide and cryopreserved until use. The viability of cryopreserved PBMCs was 60–70 %. In some patients, fresh and cryopreserved PBMCs were obtained from the same sample. To determine the frequency and phenotype of MDSCs and Tregs, multicolor fluorescence-activated cell sorting analysis was carried out using the Becton–Dickinson FACSAria II system. The following anti-human monoclonal antibodies were used: anti-CD4 (Becton–Dickinson), anti-CD11b (Becton–Dickinson), anti-CD14 (Becton–Dickinson), anti-CD15 (Becton–Dickinson), anti-CD25 (Becton–Dickinson), anti-CD33 (Becton–Dickinson), anti-CD127 (Becton–Dickinson), and anti-HLA-DR (Becton–Dickinson).

Suppression assay

$CD14^+$HLA-$DR^{-/low}$ MDSCs and $CD14^+$HLA-DR^+ cells were sorted using the Becton–Dickinson FACSAria II

system. 2×10^4 PBMCs were cultured and stimulated with 1 μg/ml plate-bound anti-CD3 (eBioscience) and 1 μg/mL soluble anti-CD28 (eBioscience) in 96-well round-bottomed plates. 24 h later, to determine the suppressive ability of MDSCs, increasing concentrations of MDSCs were added to the stimulated PBMCs. Proliferation was measured by ^{3}Hincorporation after 72 h. [^{3}H] thymidine was added, and cell proliferation was measured by incorporation of radiolabeled thymidine for 24 h.

Cytokine and chemokine profiling

Blood samples were collected from patients at the same time of PBMC isolation. After centrifugation at 3,000 rpm for 10 min at 4 °C, serum fractions were obtained and stored at −20 °C until use. Serum levels of various cytokines and chemokines were measured using the Bio-Plex Protein Array System. Briefly, frozen serum samples were thawed at room temperature and diluted 1:4 in sample diluents; 50 μl aliquots of the diluted sample was added in duplicate to the wells of 96-well microtiter plates containing the coated beads for a validated panel of human cytokines and chemokines according to the manufacturer's instructions. The following 27 cytokines and chemokines were targeted: IL-1β, IL-1 receptor antagonist (IL-1Ra), IL-2, IL-4, IL-5, IL-6, IL-7, IL-8, IL-9, IL-10, IL-12(p70), IL-13, IL-15, IL-17, basic fibroblast growth factor (FGF), eotaxin (chemokine C–C motif ligand (CCL) 11), G-CSF, GM-CSF, IFN-γ, interferon gamma-induced protein (IP)-10, monocyte chemoattractant protein (MCP)-1, macrophage inflammatory protein (MIP)-1α, MIP-1β, platelet-derived growth factor (PDGF)-BB, regulated upon activation, normal T cell expressed and secreted (RANTES), TNF-α, and vascular endothelial growth factor (VEGF). Nine standards (ranging from 0.5 to 32,000 pg/ml) were used to generate calibration curves for each cytokine. Data acquisition and analysis were performed using Bio-Plex Manager software version 4.1.1.

Statistical analysis

Data are expressed as the mean ± SD. Chi-squared test with Yates' correction, unpaired t test, Mann–Whitney U test, and Kruskal–Wallis were used for univariate analysis of two groups that were classified according to the frequency of MDSCs. The probability of tumor recurrence-free survival was estimated using the Kaplan–Meier method. The Mantel-Cox log-rank test was used to compare curves between groups. The prognostic factors for tumor recurrence-free survival were analyzed for statistical significance by the Kaplan–Meier method (univariate) and the Cox proportional hazard model (multivariate). Variables with $p < 0.1$ were entered into multivariate logistic regression analysis. A level of $p < 0.05$ was considered significant.

Results

$CD14^+HLA\text{-}DR^{-/low}$ MDSCs are increased in the peripheral blood of HCC patients

We analyzed the peripheral blood of 123 patients with HCC, 26 CLD patients without HCC, and 13 healthy donors for the prevalence of $CD14^+HLA\text{-}DR^{-/low}$ MDSCs. Because the PBMCs are tested after Ficoll, some cells may be lost. Therefore, we examined the population of MDSCs as a percentage of total $CD14^+$ cells by flow cytometry after cell surface labeling for the expression of HLA-DR (Fig. 1a). $CD14^+HLA\text{-}DR^{-/low}$ population in PBMCs of HCC patients represented 3.2–56.8 % of the $CD14^+$ cells. The frequency of $CD14^+HLA\text{-}DR^{-/low}$ MDSCs/$CD14^+$ cells in cryopreserved PBMCs correlated with that in fresh PBMCs (Fig. 1b). Therefore, we analyzed the frequency of $CD14^+HLA\text{-}DR^{-/low}$ MDSCs/$CD14^+$ cells using cryopreserved PBMCs.

To confirm the function of these cells, sorted $CD14^+HLA\text{-}DR^{-/low}$ MDSCs and $CD14^+HLA\text{-}DR^+$ (control) cells were added at different ratios to autologous anti-CD3/CD28-stimulated PBMCs, and the proliferation was measured by ^{3}Hincorporation. $CD14^+HLA\text{-}DR^{-/low}$ MDSCs of HCC patients significantly decreased autologous PBMC proliferation (Fig. 1c). On the other hand, $CD14^+HLA\text{-}DR^+$ (control) cells could not suppress the autologous PBMC proliferation.

As shown in Fig. 1d, the frequency of MDSCs was significantly higher in HCC patients (19.0 %) than in healthy donors (9.4 %) ($p < 0.01$). Overall frequencies of $CD14^+$ cells did not differ significantly between the groups (Fig. 1e). Individual frequencies of MDSCs of all the patients and healthy donors are represented as scatter plots (Fig. 2a). The frequency of MDSCs was correlated with the stage of HCC (stage III and IV: 22.3 % ($n = 46$) vs. stage I and II: 17.0 % ($n = 77$), $p < 0.01$) and was significantly higher in HCC patients than CLD patients without HCC and healthy donors. Interestingly, there was no difference between CLD patients without HCC and healthy donors. Moreover, these numbers did not change depending on the degree of fibrosis or inflammatory activity of the liver (Fig. 2b, c).

In previous reports, granulocytic MDSCs were defined in combination with several surface markers including CD14, CD15, CD11b, CD33, CD66b, and HLA-DR in several cancers. Therefore, we examined the frequency of $CD15^+CD14^-CD11b^+CD33^+$ cells in 37 HCC patients and 11 healthy donors (Suppl. figure 1A). Although there was no statistical significant difference, the frequency of

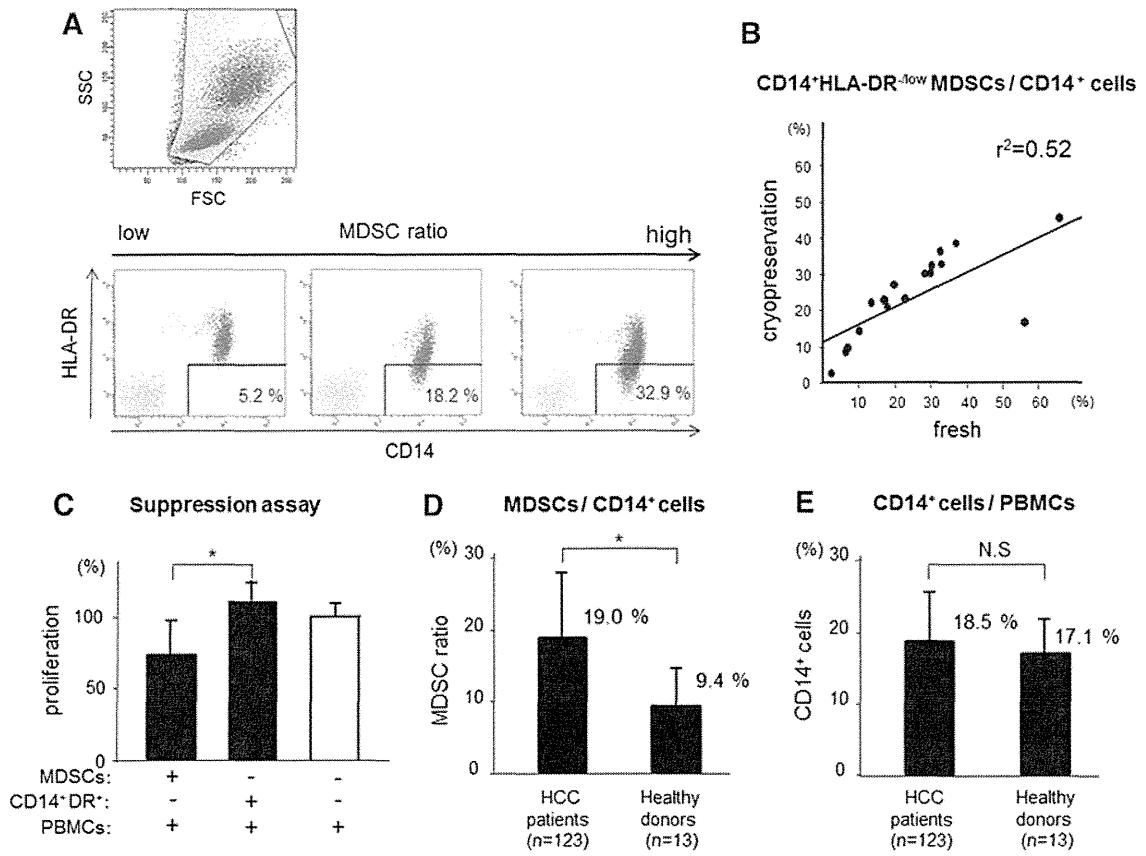

Fig. 1 **a** Flow cytometry shows $CD14^+HLA\text{-}DR^{-/low+}$ MDSCs. PBMCs from patients and healthy donors were labeled with anti-CD14 and HLA-DR. Three staining examples of HCC patients are shown in the order from a small number (*left*) to a large number (*right*). **b** The increase in $CD14^+HLA\text{-}DR^{-/low}$ MDSCs/$CD14^+$ cells in cryopreserved PBMC correlated with that in fresh PBMC ($r^2 = 0.52$). **c** Proliferation of PBMCs stimulated by anti-CD3/28 in the presence or absence of MDSCs was measured by ^{3}Hincorporation assay. $CD14^+HLA\text{-}DR^{-/low}$ MDSCs significantly decreased autologous PBMC proliferation ($n = 4$; *, $p < 0.05$). **d** The frequency of MDSCs was significantly higher in HCC patients than healthy donors (*, $p < 0.01$). **e** Overall frequencies of $CD14^+$ cells did not differ significantly

$CD15^+CD14^-CD11b^+CD33^+$ cells in HCC patients was higher than that in healthy donors (2.84 vs. 2.06 %, $p = 0.073$) (Suppl. figure 1B). The frequency was correlated with the stage of HCC (stage III and IV: 3.69 % ($n = 13$) vs. stage I and II: 2.39 % ($n = 24$), $p = 0.022$) (Suppl. figure 1C).

Relationship between the frequency of Tregs and MDSCs

It is well known that the frequency of circulating Tregs is increased and correlated with disease progression in HCC patients. The frequency of $CD4^+$ $CD25^+$ $CD127^{-/low}$ Tregs was significantly increased in HCC patients (Suppl. figure 2A) and associated with tumor progression (Suppl. figure 2B). However, there was not a strong correlation between the frequency of MDSCs and Tregs in our study (Suppl. figure 2C).

Identification of host factors related to the frequency of MDSCs in HCC patients

We divided the HCC patients into two groups using the threshold of an MDSC ratio of 22 %. This threshold is the average +2SD of the MDSC ratio in non-HCC patients. In the group with high frequency, the tumor factors including size, multiplicity, and stage were significantly worse (tumor size, 28.3 vs. 24.4 mm; tumor multiplicity (multiple/solitary), 27/12 vs. 42/42; TNM stage (I and II vs. III and IV), 17/22 vs. 60/24, $p < 0.05$) (Table 1). Moreover, hepatic reserve was also worse in the group with high frequency (Child-Pugh classification (A/B/C), 20/17/2 vs. 64/16/4, $p < 0.05$). In addition, overall survival was significantly shortened in the group with high frequency (hazard ratio 2.67, $p = 0.008$) (Suppl. figure 3A), and recurrence-free survival was also significantly shortened (hazard ratio 1.94, $p = 0.010$) (Suppl. figure 3B).

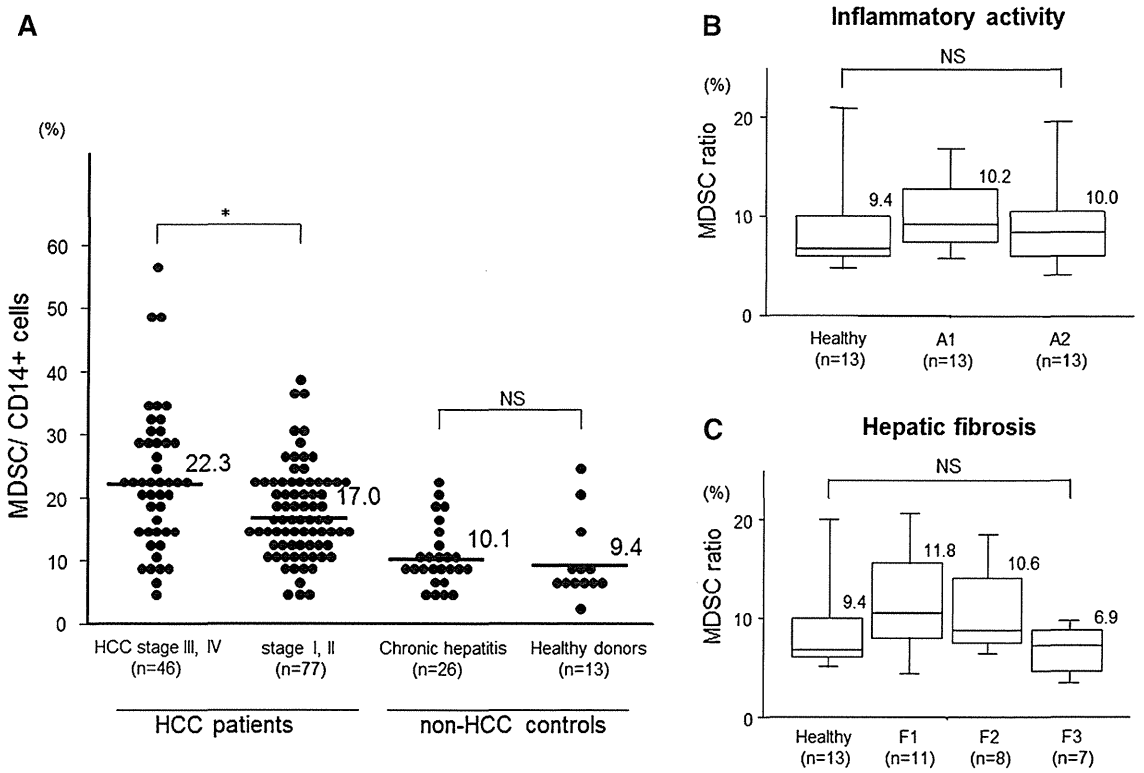

Fig. 2 **a** Scatter plots of MDSC ratio ($CD14^+HLA\text{-}DR^{-/low}$ MDSCs/ $CD14^+$ cells) in patients and healthy donors. The frequency of MDSCs was significantly increased in HCC patients compared with that in non-HCC controls. Moreover, the frequency of MDSCs was correlated with tumor progression (stage III and IV: 22.3 % ($n = 46$) vs. stage I and II: 17.0 % ($n = 77$); *, $p < 0.05$). In non-HCC controls, there was no significant difference in the frequency of MDSCs. **b**, **c** In non-HCC patients, the frequency of MDSCs did not change depending on the degree of fibrosis or inflammatory activity of the liver according to the Metavir scoring system

Relationship between serum cytokine levels and the frequency of MDSCs

In previous studies, the balance of circulating cytokines was thought to promote accumulation and activation of MDSCs [18, 31–34]. Therefore, we examined the relationship between serum cytokine levels and the frequency of MDSCs in HCC patients. In 54 HCC patients, serum levels of cytokines and chemokines were measured using the Bio-Plex Protein Array system. Serum concentrations of IL-10, IL-13, and VEGF were significantly increased in the group with a high frequency of MDSCs (Table 2). In addition, there was a positive correlation between these cytokine levels in serum and the frequency of MDSCs. We also examined the relationship between serum cytokine levels and the frequency of Tregs. We divided the HCC patients into two groups using the threshold of 7 %, which is the average +2SD of the % of Tregs among $CD4^+$ cells in non-HCC patients. Serum concentration of IL-10 was significantly increased in the group with a high frequency of Tregs (Suppl. table 2).

Kinetics of MDSCs before and after curative RFA therapy

We examined the frequency of MDSCs before and after curative RFA therapy in 33 patients. For this analysis, blood samples were obtained on the day of treatment (before) and 2–4 weeks after treatment (after). The frequency of MDSCs was significantly decreased after RFA therapy (18.0 to 15.5 %, $p < 0.05$) (Fig. 3a). However, in several patients, the frequency of MDSCs remained at a high level compared with that in non-HCC patients. The clinical parameters before RFA were not statistically different between the patients with and without a high frequency of MDSCs after RFA (Suppl. table 3).

Next, we followed up these patients for recurrence and analyzed the risk factors. If a high frequency of MDSC was observed after curative RFA therapy, the recurrence-free survival was significantly shortened (Fig. 3b). In contrast, the frequency of MDSCs before treatment did not affect the recurrence. In univariate analysis for recurrence, post-treatment MDSC ratio ≥22 % ($p = 0.023$) and tumor

Table 1 Clinical findings and MDSCs

Clinical characteristics	MDSC ratio ≥22 ($n = 39$)	MDSC ratio <22 ($n = 84$)	p value
Age (year)	68.5	70.1	0.646
Sex (M/F)	29/10	54/30	0.267
AST (IU/l)	62.0	61.5	0.543
ALT (IU/l)	47.1	53.9	0.759
LDH (IU/l)	225	218	0.832
γGTP (IU/l)	78.0	76.0	0.252
Platelet (10^4/μl)	10.9	10.6	0.884
Prothrombin time (%)	75.2	82.3	0.045
Serum albumin (g/dl)	3.53	3.68	0.120
Total bilirubin (mg/dl)	1.21	0.94	0.286
WBC (/μl)	3910	3610	0.235
Neutrophil (%)	63.2	59.4	0.093
Lymphocyte (%)	26.1	29.5	0.047
Total cholesterol (mg/dl)	151	149	0.926
HbA1c (%)	5.27	5.43	0.197
Type IV collagen 7S (ng/ml)	8.2	7.3	0.086
DCP (mAU/ml)	5157	432	0.561
AFP (ng/ml)	1301	934	0.240
Tumor size (mm)	28.3	24.4	0.014
Tumor multiplicity (multiple/solitary)	27/12	42/42	0.046
TNM stage (I plus II/III plus IV)	17/22	60/24	0.003
Child-Pugh (A/B/C)	20/17/2	64/16/4	0.015
Etiology (HCV/HBV/others)	21/11/7	61/11/12	0.081
$CD4^+$ $CD25^+$ $CD127^{-/low}$ Tregs/ $CD4^+$ cells (%)	7.04	6.70	0.281

AST aspirate aminotransferase, *ALT* alanine aminotransferase, *LDH* lactic dehydrogenase, *γGTP* gamma glutamyltransferase, *WBC* white blood cell, *Hb* hemoglobin, *DCP* des-gamma-prothrombin, *AFP* alpha-fetoprotein, *HCV* hepatitis C virus, *HBV* hepatitis B virus, *Tregs* regulatory T cells

Chi-squared test with Yates' correction, unpaired t test, Mann–Whitney U test, and Kruskal–Wallis test were used for univariate analysis of two groups that were classified according to the frequency of MDSCs

multiplicity ($p = 0.010$) were significantly associated with HCC recurrence (Table 3). In multivariable analysis for recurrence, considering the variables in the univariate analysis with $p < 0.1$, only post-treatment MDSC ratio ≥22 % (HR 3.906, $p = 0.014$) was extracted as a significant risk factor for recurrence.

Discussion

MDSCs are expanded in pathological conditions such as malignancy, infection, or trauma and consist of a heterogeneous population of immature myeloid cells [15, 25]. In pathological conditions, immature myeloid cells are blocked to differentiate into mature macrophages, dendritic cells, or granulocytes; as a result, MDSCs are accumulated [15, 25]. MDSCs strongly inhibit anti-tumor immune response through a number of mechanisms [15, 25]. As monocytic subsets of MDSCs, $CD14^+HLA\text{-}DR^{-/low}$ MDSCs have been reported in various malignancies, including melanoma, multiple myeloma, prostate cancer, and bladder cancer [18, 20, 22, 35]. In the most recent study, Hoechst et al. [24] reported that $CD14^+HLA\text{-}DR^{-/low}$ MDSCs were significantly increased in HCC patients and they suppressed T cell functions through the induction of $CD4^+CD25^+Foxp3^+$ Treg.

In the present study, in addition to an increase in the number of MDSCs in HCC patients, we observed that the frequency was correlated with the progression of HCC. Consistent with our results, it has also been reported that the frequency of $CD14^+HLA\text{-}DR^{-/low}$ MDSCs was correlated with tumor progression in patients with other cancers, such as melanoma, prostate cancer, and bladder cancer [22, 35, 36]. However, the mechanisms behind the increase in MDSCs in advanced cancer patients are still unclear. As is well known, there is a close relationship between hepatocarcinogenesis and histological status of underlying liver [37, 38]. Therefore, the advance of hepatic fibrosis and the increase in inflammatory cell infiltration into liver might result in an increase in MDSCs following the progression of HCC. However, there was no relationship between the frequency of $CD14^+HLA\text{-}DR^{-/low}$ MDSCs and underlying liver status in our study. From our observations, increase in MDSCs was only correlated with tumor progression, but not with hepatic fibrosis or disease activity of CLD. This finding suggests that the expansion of $CD14^+HLA\text{-}DR^{-/low}$ MDSCs was mostly derived from the tumor environment itself, but not from inflammation or fibrosis of liver tissue around the tumor. The finding that a significant decrease in the frequency of circulating $CD14^+HLA\text{-}DR^{-/low}$ MDSCs is observed in most patients with curative treatment in this study supports this hypothesis. On the other hand, Tregs were also increased in HCC patients and associated with the progression of HCC. Though it was reported that MDSCs suppressed T cell function through the induction of Tregs, there was not a strong correlation between the frequencies of these two immunosuppressive cells.

Regarding the mechanism of MDSC expansion, we also analyzed the relationship between the serum cytokine levels and the frequency of MDSCs. We observed that the serum concentrations of IL-10, IL-13, and VEGF were significantly increased in the group with high frequency of MDSCs and there was a positive correlation between these cytokine levels and the frequency of MDSCs. Moreover, although there was no significant difference, the serum

Table 2 Serum cytokines and MDSCs

Cytokine	Healthy donor (mean) ($n = 13$)	MDSC ratio ≥ 22 (mean) ($n = 21$)	Range	MDSC ratio < 22 (mean) ($n = 31$)	Range	p value
IL-1ra	34.2	97.0	(21.5–600)	40.3	(3.4–151)	0.057
IL-2	10.5	38.1	(4.3–54.3)	11.3	(0.9–49.7)	0.055
IL-4	2.6	5.75	(1.47–11.9)	5.03	(0.71–10.9)	0.159
IL-6	9.9	21.5	(1.2–130)	10.1	(0.2–97.2)	0.065
IL-8	24.5	64.7	(10.9–291)	35.1	(6.2–142)	0.156
IL-10	2.76	6.01	(0.8–11.5)	2.81	(0.1–12.0)	0.003
IL-12(p70)	14.6	33.3	(0.6–140)	17.6	(1.4–57)	0.058
IL-13	7.6	13.1	(1.2–33.6)	8.2	(2.7–22.9)	0.015
IL-17	15.7	23.5	(4.6–70)	20.8	(2.1–119)	0.115
Eotaxin	104	141	(51.9–493)	124	(26.3–331)	0.675
G-CSF	7.9	13.2	(2.7–41.3)	8.7	(0.5–17.9)	0.050
IFN-γ	52.6	95.4	(23.1–417)	69.9	(2.5–238)	0.136
MCP-1	20.2	26.8	(8.4–114)	23.8	(3.5–77)	0.744
MIP-1b	97.6	120	(58.3–490)	108	(39.7–263)	0.508
PDGF	4012	4375	(1,312–10,136)	4013	(831–13,557)	0.484
RANTES	2978	2890	(1,040–4,826)	3184	(599–6,165)	0.186
TNF-α	10.5	34.9	(0.1–175)	27.6	(2.9–105)	0.756
VEGF	34.6	101.7	(22.5–371)	59.5	(9.3–183)	0.045

IL interleukin, *G-CSF* granulocytic colony stimulating factor, *IFN* interferon, *MCP* monocyte chemoattractant protein, *MIP* macrophage inflammatory protein, *PDGF* platelet-derived growth factor, *RANTES* regulated upon activation, normal T cell expressed and secreted, *TNF* tumor necrosis factor, *VEGF* vascular endothelial growth factor

Mann–Whitney *U* test was used for univariate analysis of two groups that were classified according to the frequency of MDSCs

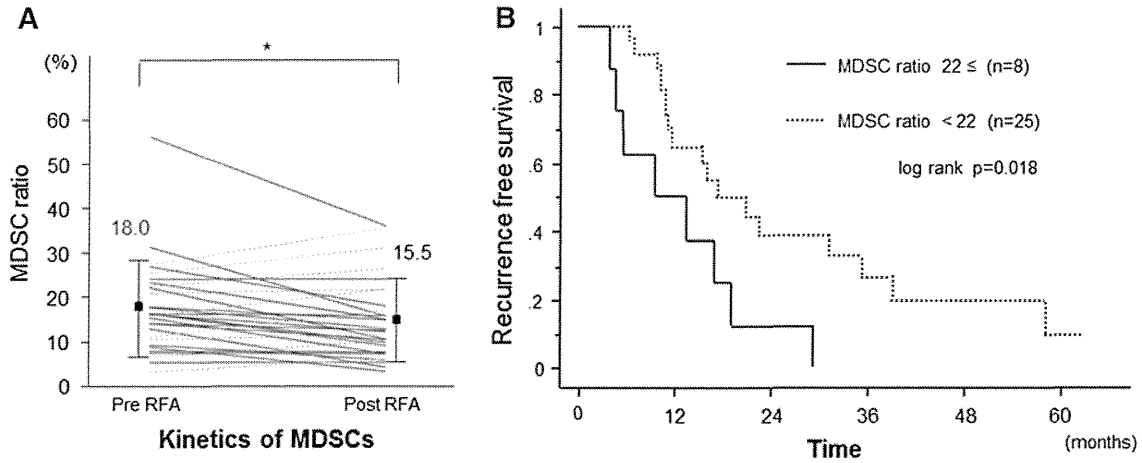

Fig. 3 **a** In 33 HCC patients who received curative RFA therapy, the frequency of MDSCs was significantly decreased after treatment. However, in several patients, the frequencies were increased after treatment (*dotted lines*) (*, $p < 0.05$). **b** Kaplan–Meier curve for recurrence-free survival after RFA therapy. The patients with high frequency of MDSCs (*solid line*) relapsed

concentrations of IL-1ra, IL-2, IL-6, IL-12(p70), and G-CSF tended to be increased in the group with high frequency of MDSCs. In accordance with our results, various cytokines, including IL-6, IL-10, IL-13, G-CSF, and VEGF, that trigger Janus kinase (JAK)-signal transducer and activator of transcription (STAT) signaling pathways have been reported to be associated with the frequency of MDSCs [39]. In particular, the cytokines involved in the JAK2-STAT3 signaling pathway are considered to be the main regulators of the expansion of MDSCs, which leads to stimulation of myelopoiesis and inhibition of myeloid-cell differentiation [40–42].

Table 3 Cox proportional hazards regression for recurrence

Variant	Univariate HR (95 % CI)	*p* value	Multivariable HR (95 % CI)	*p* value
Sex: female	0.763 (0.446–1.308)	0.326		
Age: ≥70 years	1.111 (0.671–1.840)	0.683		
Pre-MDSC ratio: ≥22 %	1.210 (0.698–2.096)	0.497		
Pre-neutrophil	0.990 (0.969–1.012)	0.385		
Pre-lymphocyte	1.014 (0.987–1.043)	0.311		
Pre-neutrophil/lymphocyte	0.978 (0.787–1.216)	0.844		
Pre-ALT	1.001 (0993–1.008)	0.882		
Pre-serum albumin: <3.5 mg/dl	1.143 (0.665–1.982)	0.647		
Pre-prothrombin time: <70 %	1.662 (0.961–2.903)	0.073	1.881 (0.522–6.777)	0.101
Post-MDSC ratio: ≥22 %	2.795 (1.150–6.792)	0.023	3.906 (1.313–11.616)	0.014
Post-neutrophil	1.005 (0.975–1.035)	0.762		
Post-lymphocyte	0.993 (0.960–1.027)	0.678		
Post-neutrophil/lymphocyte	1.003 (0.810–1.242)	0.980		
Post-ALT	0.995 (0.981–1.010)	0.501		
Type IV collagen 7S	1.122 (0.992–1.268)	0.067	1.192 (0.907–1.566)	0.207
AFP: ≥100 ng/ml	1.357 (0.743–2.480)	0.321		
Tumor size: ≥20 mm	1.29 (0.78–2.12)	0.328		
Tumor multiplicity: multiple	2.00 (1.18–3.40)	0.010	1.851 (0.721–4.753)	0.201

HR hazard ratio, *CI* confidence interval, *ALT* alanine aminotransferase, *AFP* alpha-fetoprotein

Another important finding of our study is that the frequency of MDSCs showed various changes after curative RFA and this frequency is an independent risk factor of HCC recurrence. In most of the patients, the frequency of MDSCs decreased after RFA. A similar phenomenon has also been reported in other cancer treatments [19, 21, 36]. Liu et al. [21] reported that MDSCs were decreased in non-small cell lung cancer patients who had clinical benefit from chemotherapy or who received curative surgery. These results suggest that a decrease in the frequency of MDSCs is due to tumor eradication.

It is well known that tumor factors including multiplicity, tumor diameter, serum levels of tumor marker, and hepatic reserve are risk factors of HCC recurrence after RFA [43, 44], but it has not been reported that the frequency of circulating MDSCs is also a risk factor. From our findings, there was a clear inverse correlation between the frequency of MDSCs after RFA and recurrence-free survival. Consistent with our results, in the patients with pancreatic, esophageal, and gastric cancer, Gabitass et al. [23] reported that an increase in MDSCs was associated with an increased risk of death and that the frequency of MDSCs was an independent prognostic factor for patient survival. Taken together with these findings, our results suggest that the frequency of MDSCs might be one of the prognostic factors of patients after cancer treatments.

As we showed, the frequency of MDSCs is primarily correlated with tumor progression. However, between the patients with high and low frequency of MDSCs after RFA, there was no significant difference in hepatic reserve and tumor factors before treatment. Although an incomplete HCC eradication at a microscopic level may allow a high frequency of MDSCs after RFA, there may be other mechanisms such as subsequently tumor-specific immune responses after RFA. In addition, there is a limitation of the present study because we used cryopreserved PBMCs for phenotypic analysis of MDSCs. Further studies using fresh PBMCs are needed for precise phenotypic analysis of MDSCs and elucidation of the mechanism to regulate the frequency of MDSCs after HCC treatment.

In conclusion, the frequency of MDSCs in HCC patients is correlated with tumor progression, and the frequency after RFA is inversely correlated with the prognosis of HCC patients. HCC patients who show a high frequency of MDSCs after RFA should be closely followed, and the inhibition or elimination of MDSCs after HCC treatments may improve the prognosis of HCC patients.

Acknowledgments This study was supported by research grants from the Ministry of Education, Culture, Sports, Science and Technology of Japan.

Conflict of interest The authors declare no conflict of interest.

References

1. Thomas MB, Jaffe D, Choti MM, Belghiti J, Curley S, Fong Y, Gores G (2010) Hepatocellular carcinoma: consensus recommendations of the National Cancer Institute Clinical Trials Planning Meeting. J Clin Oncol 28:3994–4005

2. Llovet JM, Burroughs A, Bruix J (2003) Hepatocellular carcinoma. Lancet 362:1907–1917
3. Lencioni R, Chen XP, Dagher L, Venook AP (2010) Treatment of intermediate/advanced hepatocellular carcinoma in the clinic: how can outcomes be improved? Oncologist 15 Suppl 4:42–52
4. Curley SA, Izzo F, Ellis LM, Nicolas Vauthey J, Vallone P (2000) Radiofrequency ablation of hepatocellular cancer in 110 patients with cirrhosis. Ann Surg 232:381–391
5. Ishizaki Y, Kawasaki S (2008) The evolution of liver transplantation for hepatocellular carcinoma (past, present, and future). J Gastroenterol 43:18–26
6. Yamashita T, Arai K, Sunagozaka H, Ueda T, Terashima T, Mizukoshi E, Sakai A (2011) Randomized, phase II study comparing interferon combined with hepatic arterial infusion of fluorouracil plus cisplatin and fluorouracil alone in patients with advanced hepatocellular carcinoma. Oncology 81:281–290
7. Llovet JM, Ricci S, Mazzaferro V, Hilgard P, Gane E, Blanc JF, de Oliveira AC (2008) Sorafenib in advanced hepatocellular carcinoma. N Engl J Med 359:378–390
8. Butterfield LH (2004) Immunotherapeutic strategies for hepatocellular carcinoma. Gastroenterology 127:S232–S241
9. Sun K, Wang L, Zhang Y (2006) Dendritic cell as therapeutic vaccines against tumors and its role in therapy for hepatocellular carcinoma. Cell Mol Immunol 3:197–203
10. Zerbini A, Pilli M, Penna A, Pelosi G, Schianchi C, Molinari A, Schivazappa S (2006) Radiofrequency thermal ablation of hepatocellular carcinoma liver nodules can activate and enhance tumor-specific T-cell responses. Cancer Res 66:1139–1146
11. Palmer DH, Midgley RS, Mirza N, Torr EE, Ahmed F, Steele JC, Steven NM (2009) A phase II study of adoptive immunotherapy using dendritic cells pulsed with tumor lysate in patients with hepatocellular carcinoma. Hepatology 49:124–132
12. Mizukoshi E, Nakamoto Y, Arai K, Yamashita T, Sakai A, Sakai Y, Kagaya T (2011) Comparative analysis of various tumor-associated antigen-specific t-cell responses in patients with hepatocellular carcinoma. Hepatology 53:1206–1216
13. Whiteside TL (2006) Immune suppression in cancer: effects on immune cells, mechanisms and future therapeutic intervention. Semin Cancer Biol 16:3–15
14. Khattri R, Cox T, Yasayko SA, Ramsdell F (2003) An essential role for Scurfin in CD4 + CD25 + T regulatory cells. Nat Immunol 4:337–342
15. Gabrilovich DI, Nagaraj S (2009) Myeloid-derived suppressor cells as regulators of the immune system. Nat Rev Immunol 9:162–174
16. Zea AH, Rodriguez PC, Atkins MB, Hernandez C, Signoretti S, Zabaleta J, McDermott D (2005) Arginase-producing myeloid suppressor cells in renal cell carcinoma patients: a mechanism of tumor evasion. Cancer Res 65:3044–3048
17. Gordon IO, Freedman RS (2006) Defective antitumor function of monocyte-derived macrophages from epithelial ovarian cancer patients. Clin Cancer Res 12:1515–1524
18. Filipazzi P, Valenti R, Huber V, Pilla L, Canese P, Iero M, Castelli C (2007) Identification of a new subset of myeloid suppressor cells in peripheral blood of melanoma patients with modulation by a granulocyte-macrophage colony-stimulation factor-based antitumor vaccine. J Clin Oncol 25:2546–2553
19. Diaz-Montero CM, Salem ML, Nishimura MI, Garrett-Mayer E, Cole DJ, Montero AJ (2009) Increased circulating myeloid-derived suppressor cells correlate with clinical cancer stage, metastatic tumor burden, and doxorubicin-cyclophosphamide chemotherapy. Cancer Immunol Immunother 58:49–59
20. Brimnes MK, Vangsted AJ, Knudsen LM, Gimsing P, Gang AO, Johnsen HE, Svane IM (2010) Increased level of both CD4 + FOXP3 + regulatory T cells and CD14 + HLA-DR$^-$/low myeloid-derived suppressor cells and decreased level of dendritic cells in patients with multiple myeloma. Scand J Immunol 72:540–547
21. Liu CY, Wang YM, Wang CL, Feng PH, Ko HW, Liu YH, Wu YC (2010) Population alterations of L-arginase- and inducible nitric oxide synthase-expressed CD11b +/CD14$^-$/CD15 +/CD33 + myeloid-derived suppressor cells and CD8 + T lymphocytes in patients with advanced-stage non-small cell lung cancer. J Cancer Res Clin Oncol 136:35–45
22. Vuk-Pavlović S, Bulur PA, Lin Y, Qin R, Szumlanski CL, Zhao X, Dietz AB (2010) Immunosuppressive CD14 + HLA-DRlow/- monocytes in prostate cancer. Prostate 70:443–455
23. Gabitass RF, Annels NE, Stocken DD, Pandha HA, Middleton GW (2011) Elevated myeloid-derived suppressor cells in pancreatic, esophageal and gastric cancer are an independent prognostic factor and are associated with significant elevation of the Th2 cytokine interleukin-13. Cancer Immunol Immunother 60:1419–1430
24. Hoechst B, Ormandy LA, Ballmaier M, Lehner F, Krüger C, Manns MP, Greten TF (2008) A new population of myeloid-derived suppressor cells in hepatocellular carcinoma patients induces CD4(+)CD25(+)Foxp3(+) T cells. Gastroenterology 135:234–243
25. Ostrand-Rosenberg S, Sinha P (2009) Myeloid-derived suppressor cells: linking inflammation and cancer. J Immunol 182:4499–4506
26. Youn JI, Nagaraj S, Collazo M, Gabrilovich DI (2008) Subsets of myeloid-derived suppressor cells in tumor-bearing mice. J Immunol 181:5791–5802
27. Greten TF, Manns MP, Korangy F (2011) Myeloid derived suppressor cells in human diseases. Int Immunopharmacol 11:802–807
28. Filipazzi P, Huber V, Rivoltini L (2011) Phenotype, function and clinical implications of myeloid-derived suppressor cells in cancer patients. Cancer Immunol Immunother 61(2):255–263
29. Ormandy LA, Hillemann T, Wedemeyer H, Manns MP, Greten TF, Korangy F (2005) Increased populations of regulatory T cells in peripheral blood of patients with hepatocellular carcinoma. Cancer Res 65:2457–2464
30. Fu J, Xu D, Liu Z, Shi M, Zhao P, Fu B, Zhang Z (2007) Increased regulatory T cells correlate with CD8 T-cell impairment and poor survival in hepatocellular carcinoma patients. Gastroenterology 132:2328–2339
31. Kusmartsev S, Gabrilovich DI (2006) Effect of tumor-derived cytokines and growth factors on differentiation and immune suppressive features of myeloid cells in cancer. Cancer Metastasis Rev 25:323–331
32. Bunt SK, Sinha P, Clements VK, Leips J, Ostrand-Rosenberg S (2006) Inflammation induces myeloid-derived suppressor cells that facilitate tumor progression. J Immunol 176:284–290
33. Bunt SK, Yang L, Sinha P, Clements VK, Leips J, Ostrand-Rosenberg S (2007) Reduced inflammation in the tumor microenvironment delays the accumulation of myeloid-derived suppressor cells and limits tumor progression. Cancer Res 67:10019–10026
34. Lechner MG, Liebertz DJ, Epstein AL (2010) Characterization of cytokine-induced myeloid-derived suppressor cells from normal human peripheral blood mononuclear cells. J Immunol 185:2273–2284
35. Yuan XK, Zhao XK, Xia YC, Zhu X, Xiao P (2011) Increased circulating immunosuppressive CD14(+)HLA-DR(-/low) cells correlate with clinical cancer stage and pathological grade in patients with bladder carcinoma. J Int Med Res 39:1381–1391
36. Poschke I, Mougiakakos D, Hansson J, Masucci GV, Kiessling R (2010) Immature immunosuppressive CD14 + HLA-DR-/low cells in melanoma patients are Stat3hi and overexpress CD80, CD83, and DC-sign. Cancer Res 70:4335–4345

37. Fattovich G, Stroffolini T, Zagni I, Donato F (2004) Hepatocellular carcinoma in cirrhosis: incidence and risk factors. Gastroenterology 127:S35–S50
38. El-Serag HB, Rudolph KL (2007) Hepatocellular carcinoma: epidemiology and molecular carcinogenesis. Gastroenterology 132:2557–2576
39. Bromberg J (2002) Stat proteins and oncogenesis. J Clin Invest 109:1139–1142
40. Nefedova Y, Huang M, Kusmartsev S, Bhattacharya R, Cheng P, Salup R, Jove R (2004) Hyperactivation of STAT3 is involved in abnormal differentiation of dendritic cells in cancer. J Immunol 172:464–474
41. Yu H, Kortylewski M, Pardoll D (2007) Crosstalk between cancer and immune cells: role of STAT3 in the tumour microenvironment. Nat Rev Immunol 7:41–51
42. Cheng P, Corzo CA, Luetteke N, Yu B, Nagaraj S, Bui MM, Ortiz M (2008) Inhibition of dendritic cell differentiation and accumulation of myeloid-derived suppressor cells in cancer is regulated by S100A9 protein. J Exp Med 205:2235–2249
43. Izumi N, Asahina Y, Noguchi O, Uchihara M, Kanazawa N, Itakura J, Himeno Y (2001) Risk factors for distant recurrence of hepatocellular carcinoma in the liver after complete coagulation by microwave or radiofrequency ablation. Cancer 91:949–956
44. Komorizono Y, Oketani M, Sako K, Yamasaki N, Shibatou T, Maeda M, Kohara K (2003) Risk factors for local recurrence of small hepatocellular carcinoma tumors after a single session, single application of percutaneous radiofrequency ablation. Cancer 97:1253–1262

Histidine Augments the Suppression of Hepatic Glucose Production by Central Insulin Action

Kumi Kimura,[1] Yusuke Nakamura,[1] Yuka Inaba,[1] Michihiro Matsumoto,[2] Yoshiaki Kido,[3,4] Shun-ichiro Asahara,[3] Tomokazu Matsuda,[3] Hiroshi Watanabe,[5] Akifumi Maeda,[5] Fuyuhiko Inagaki,[6] Chisato Mukai,[6] Kiyoshi Takeda,[7] Shizuo Akira,[8] Tsuguhito Ota,[9] Hajime Nakabayashi,[10] Shuichi Kaneko,[11] Masato Kasuga,[12] and Hiroshi Inoue[1]

Glucose intolerance in type 2 diabetes is related to enhanced hepatic glucose production (HGP) due to the increased expression of hepatic gluconeogenic enzymes. Previously, we revealed that hepatic STAT3 decreases the expression of hepatic gluconeogenic enzymes and suppresses HGP. Here, we show that increased plasma histidine results in hepatic STAT3 activation. Intravenous and intracerebroventricular (ICV) administration of histidine-activated hepatic STAT3 reduced G6Pase protein and mRNA levels and augmented HGP suppression by insulin. This suppression of hepatic gluconeogenesis by histidine was abolished by hepatic STAT3 deficiency or hepatic Kupffer cell depletion. Inhibition of HGP by histidine was also blocked by ICV administration of a histamine H_1 receptor antagonist. Therefore, histidine activates hepatic STAT3 and suppresses HGP via central histamine action. Hepatic STAT3 phosphorylation after histidine ICV administration was attenuated in histamine H_1 receptor knockout (Hrh1KO) mice but not in neuron-specific insulin receptor knockout (NIRKO) mice. Conversely, hepatic STAT3 phosphorylation after insulin ICV administration was attenuated in NIRKO but not in Hrh1KO mice. These findings suggest that central histidine action is independent of central insulin action, while both have additive effects on HGP suppression. Our results indicate that central histidine/histamine-mediated suppression of HGP is a potential target for the treatment of type 2 diabetes. ***Diabetes* 62:2266–2277, 2013**

From the [1]Department of Physiology and Metabolism, Brain/Liver Interface Medicine Research Center, Kanazawa University, Kanazawa, Japan; the [2]Department of Molecular Metabolic Regulation, Diabetes Research Center, Research Institute, National Center for Global Health and Medicine, Tokyo, Japan; the [3]Division of Diabetes and Endocrinology, Kobe University Graduate School of Medicine, Kobe, Japan; the [4]Division of Analytical Biomedical Sciences, Kobe University Graduate School of Health Sciences, Kobe, Japan; [5]BRAND'S Brain Research Centre, Cerebos Pacific Limited, Singapore, Singapore; the [6]Division of Pharmaceutical Sciences, Graduate School of Medical Sciences, Kanazawa University, Kanazawa, Japan; the [7]Laboratory of Immune Regulation, Department of Microbiology and Immunology, Graduate School of Medicine, Osaka University, Suita, Japan; the [8]Laboratory of Host Defense, Immunology Frontier Research Center, Department of Host Defense, Research Institute for Microbial Diseases, Osaka University, Suita, Japan; the [9]Department of Cell Metabolism and Nutrition, Brain/Liver Interface Medicine Research Center, Kanazawa University, Kanazawa, Japan; the [10]Health Science Service Center, Kanazawa University, Kanazawa, Japan; the [11]Department of Disease Control and Homeostasis, Graduate School of Medical Sciences, Kanazawa University, Kanazawa, Japan; and the [12]Diabetes Research Center, Research Institute, National Center for Global Health and Medicine, Tokyo, Japan.

Corresponding author: Hiroshi Inoue, inoue-h@staff.kanazawa-u.ac.jp.

Received 7 December 2012 and accepted 4 March 2013.

DOI: 10.2337/db12-1701

This article contains Supplementary Data online at http://diabetes.diabetesjournals.org/lookup/suppl/doi:10.2337/db12-1701/-/DC1.

Increased glucose production in type 2 diabetes is caused by elevated gluconeogenesis in the liver (1), while in actual clinical settings, treatment for diabetes includes remedies, such as metformin, that suppress hepatic gluconeogenesis (2). Hepatic gluconeogenesis is controlled by regulating the gene expression of gluconeogenic enzymes, such as phosphoenolpyruvate carboxykinase (PEPCK) and glucose-6-phosphatase (G6Pase) (2). In fact, gene expression of hepatic gluconeogenic enzymes is upregulated in obese animal models of diabetes, including *db/db* mice lacking leptin receptors (3,4), while suppression of gluconeogenic gene expression improves glucose tolerance in *db/db* mice (4–6).

Hormonal and nutrient changes regulate the expression of hepatic gluconeogenic genes by a central-mediated mechanism in addition to direct hepatic action (7,8). Insulin, the most important regulatory factor in gluconeogenesis, suppresses hepatic gluconeogenic gene expression via a central indirect mechanism through brain insulin receptors and via direct action on hepatic insulin receptors (9,10). In rodent studies, the intracerebroventricular (ICV) administration of insulin downregulates gluconeogenic gene expression in the liver and suppresses hepatic glucose production (HGP) (10,11). Conversely, HGP is increased in hypothalamic insulin receptor knockdown rats and neuron-specific insulin receptor knockout (NIRKO) mice (9,10). In addition, inhibition of phosphatidylinositol 3-kinase (PI3-K) in the insulin-signaling pathway in the hypothalamus inhibits the central insulin-dependent suppression of HGP (10). Previously, we revealed the importance of signal transducer and activator of transcription-3 (STAT3) in the central insulin-mediated suppression of gluconeogenesis in the liver. In fact, STAT3 is activated through phosphorylation, which is induced by glucose load in an insulin-dependent manner and also by the ICV administration of insulin (9). Further, liver-specific STAT3-deficient (LST3KO) mice exhibit a defect in the central insulin-mediated suppression of HGP (9), suggesting that hepatic STAT3 plays an important role in this process (9). We also revealed that the upregulation of liver-specific interleukin-6 (IL-6) expression is required for the activation of hepatic STAT3 by central insulin (9).

Changes in nutrients are known to affect hepatic gluconeogenesis via central action similarly to insulin (7,8). Glucose and long-chain fatty acids are known to suppress glucose production in the liver after ICV injection (12,13). Recent studies have reported that plasma amino acid levels are also closely associated with glucose metabolism. In fact, in individuals without diabetes and those with new-onset type 2 diabetes, fasting and 2-h blood glucose levels

after glucose loading correlate positively with the blood concentration of branched-chain amino acids alanine, phenylalanine, and tyrosine and negatively with the concentration of histidine and glutamine (14). However, the function of these amino acids in the central-mediated regulation of gluconeogenesis remains to be fully elucidated, while the branched-chain amino acid leucine reportedly suppresses HGP when administered to the hypothalamus (15). In the current study, we found that plasma histidine acts as a nutrient that suppresses hepatic gluconeogenesis via central-mediated hepatic STAT3 activation.

RESEARCH DESIGN AND METHODS

Experiments using mice were conducted in accordance with the guidelines for the care and use of laboratory animals of Kanazawa University. Male mice (8–10 weeks old) were housed under a 12-h light-dark cycle with free access to food and water. Wild-type C57BL/6J Slc mice were purchased from Japan SLC (Shizuoka, Japan), and histamine H_1 receptor knockout (Hrh1KO) (16) mice were from Oriental Bio Service (Kyoto, Japan). We generated LST3KO mice by crossing albumin-cre and floxed-STAT3 mice (5), while NIRKO mice were generated by crossing Nestin-cre and floxed–insulin receptor mice (17). Floxed-STAT3 and floxed–insulin receptor mice were used as the corresponding controls.

Administration of protein extracts and amino acids. Chicken meat extract was prepared as a protein source for gavage administration. Shredded chicken meat was cooked in a pressure cooker for 270 min and strained, the lipids were removed by centrifugation, and the protein concentration was adjusted. Snakehead fish meat was processed in the same way and used as a low-histidine (Low-His) protein source that did not increase blood histidine levels. After 16 h of fasting, the mice were orally administered protein at 2 g/kg body wt via a feeding tube. Histidine or each amino acid was administered at 0.5 mmol/kg body wt i.p. or intravenously at the concentrations shown in Figs. 2*A* and 5*G* after a 16-h fast.

Tolerance tests and biochemical and endocrine testing. A glucose, pyruvate, or fructose tolerance test was performed after a 16-h fast. For the glucose tolerance test, histidine was injected intraperitoneally at 5 min before injection of 2 g/kg body wt glucose (Otsuka Pharmaceutical, Tokushima, Japan). For the pyruvate or fructose tolerance test, histidine was injected twice at 120 and 5 min before 1 g/kg body wt sodium pyruvate or fructose, respectively (Sigma-Aldrich, St. Louis, MO). Blood glucose levels were measured using a GLUCOCARD G+ Meter (Arkray, Kyoto, Japan). Blood insulin and IL-6 levels were measured using a Mouse Insulin ELISA kit (Shibayagi, Gunma, Japan) or a Quantikine Mouse IL-6 ELISA kit (R&D Systems, Minneapolis, MN). Plasma levels of amino acids were quantified using high-performance liquid chromatography. Hypothalamic histamine levels were measured using a Histamine EIA kit (Bertin Pharma, York, U.K.). Hepatic glycogen levels were measured by the anthrone–sulfuric acid method.

Euglycemic clamp technique. Hyperinsulinemic-euglycemic clamping was performed by injecting the awake and unrestrained mice with human insulin (Eli Lilly, Indianapolis, IN) after a 16-h fast. Blood glucose levels were measured every 10 min and maintained between 90 and 120 mg/dL after intravenous insulin injections were started. Further, between 90 and 120 min after starting insulin administration, we stabilized blood glucose volatility with 20 mg/dL insulin (Supplementary Table 1). We measured the glucose infusion rate (GIR) and plasma [^{3}H]glucose specific activity every 10 min. The R_d under steady-state conditions for plasma glucose concentration was determined from the rate of [^{3}H]glucose infusion divided by the plasma [^{3}H]glucose specific activity. The rate of HGP was obtained from the difference between R_d and GIR. An internal cannula (Plastics One, Roanoke, VA) was inserted into the lateral ventricle, followed by intravenous cannulation 7–10 days later. After 4–6 days of recovery and habituation, a hyperinsulinemic-euglycemic clamp or pancreatic clamp was performed with ICV administration. After a 16-h fast, the mice received an ICV administration of human insulin, histidine, or pyrilamine with an intravenous injection of human insulin and somatostatin, as shown in Fig. 7*A*. Blood glucose levels were maintained between 90 and 120 mg/dL. The mice received 10 nmol/mouse LY294002 (Calbiochem, San Diego, CA), 50 μg/mouse pyrilamine (Wako, Osaka, Japan), 50 nmol/mouse thioperamide (Sigma), pyridylethylamine (TOCRIS Bioscience, Ellisville, MO), or artificial cerebrospinal fluid via the lateral ventricle. For the hyperinsulinemic-euglycemic clamp, pyrilamine was administered to the lateral ventricle (Fig. 5G).

IL-6 neutralizing antibody and Kupffer cell depletion. An IL-6 neutralizing antibody and control IgG (R&D Systems) were injected as previously described (9). Clodronate (LKT Laboratories, St. Paul, MN) was encapsulated into empty liposomes (NOF, Tokyo, Japan), and clodronate-containing liposomes (CLDs) were injected into the mice via the tail vein for two consecutive days to deplete Kupffer cells in the liver. The control mice received empty liposomes. Immunostaining with an anti-Mac-2 antibody (Cedarlane Laboratories, Burlington, Ontario, Canada) was performed to visualize the Kupffer cells.

Western blotting and quantitative PCR. Mouse hepatocytes were isolated as previously described (6). Immunoblotting was performed using anti–phosphorylated (phospho)-STAT3 (Tyr705), anti–phospho-Akt (Thr308), anti–phospho-p70 S6 kinase (Thr389), anti–p70 S6 kinase, anti–phospho-S6 ribosomal protein (Ser235/236), and anti-S6 ribosomal protein antibodies from Cell Signaling Technology (Danvers, MA); anti-STAT3, anti-Akt, anti–G6Pase-α, anti-PEPCK, and anti–insulin receptor β antibodies from Santa Cruz Biotechnology (Santa Cruz, CA); and an anti–β-actin antibody from Sigma. Immunoblot images were representative of at least three independent immunoblot analyses and quantified by densitometry on an LAS-3000 Imager (Fujifilm, Tokyo, Japan).

The results of quantitative PCR were analyzed using the *36B4* gene as an internal control. The primer sequences used in this study are available upon request.

Statistical analysis. Statistical analysis was performed using Student t test and one- or two-way ANOVA followed by post hoc tests, and differences were considered significant for P values <0.05.

RESULTS

Improvement of glucose tolerance after histidine administration. Phosphorylation of hepatic Akt and STAT3 was increased at 120 min after the oral administration of the protein extract (Fig. 1*A*). As in our previous study (9), glucose loading activated hepatic Akt and STAT3, suggesting that both the hepatic and central actions of insulin were induced by glucose loading. In addition, protein administration also augmented the activation of these molecules by glucose loading (Fig. 1*A*). The intake of proteins is known to facilitate the secretion of insulin (18); in fact, the continuous administration of somatostatin, which suppresses the secretion of endogenous insulin, kept Akt phosphorylation at a virtually undetectable level after ingestion of the protein extract (Fig. 1*B*), whereas protein intake increased STAT3 phosphorylation even in the presence of somatostatin (Fig. 1*B*). These findings suggest that hepatic STAT3 activation associated with protein intake is independent of the secretion of endogenous insulin. Because blood amino acid levels are increased after the oral administration of proteins (19), we administered individual amino acids intraperitoneally to investigate the effects of blood amino acid levels on hepatic STAT3 activation. We found that the hepatic STAT3 phosphorylation was increased by the administration of histidine and histidine-related amino acids and dipeptides, such as 1-methyl-histidine, β-alanyl-histidine (carnosine), and β-alanyl-1-methyl-histidine (anserine) (Fig. 1*C*). Therefore, we investigated the importance of histidine and histidine-containing dipeptides in the activation of hepatic STAT3 using a protein and Low-His protein extract. Coincident with the plasma concentration of histidine and other histidine-containing dipeptides (Supplementary Table 2), a milder increase in STAT3 phosphorylation was observed in the Low-His group compared with the protein group (Fig. 1*D*).

Because histidine administration activates hepatic STAT3, we then conducted a glucose tolerance test to investigate the role of histidine in glucose homeostasis. With the intraperitoneal administration of 500 μmol/kg body wt histidine, which maintained the blood concentration of histidine close to that obtained after the oral administration of 2 g/kg body wt protein (Supplementary Table 3), blood glucose levels were significantly decreased at 120 min after glucose loading (Fig. 1*E*). Conversely, there was no change in plasma insulin levels after histidine administration (Fig. 1*F*). Phosphorylation of hepatic STAT3 increased at 120 min after histidine administration, which was further increased

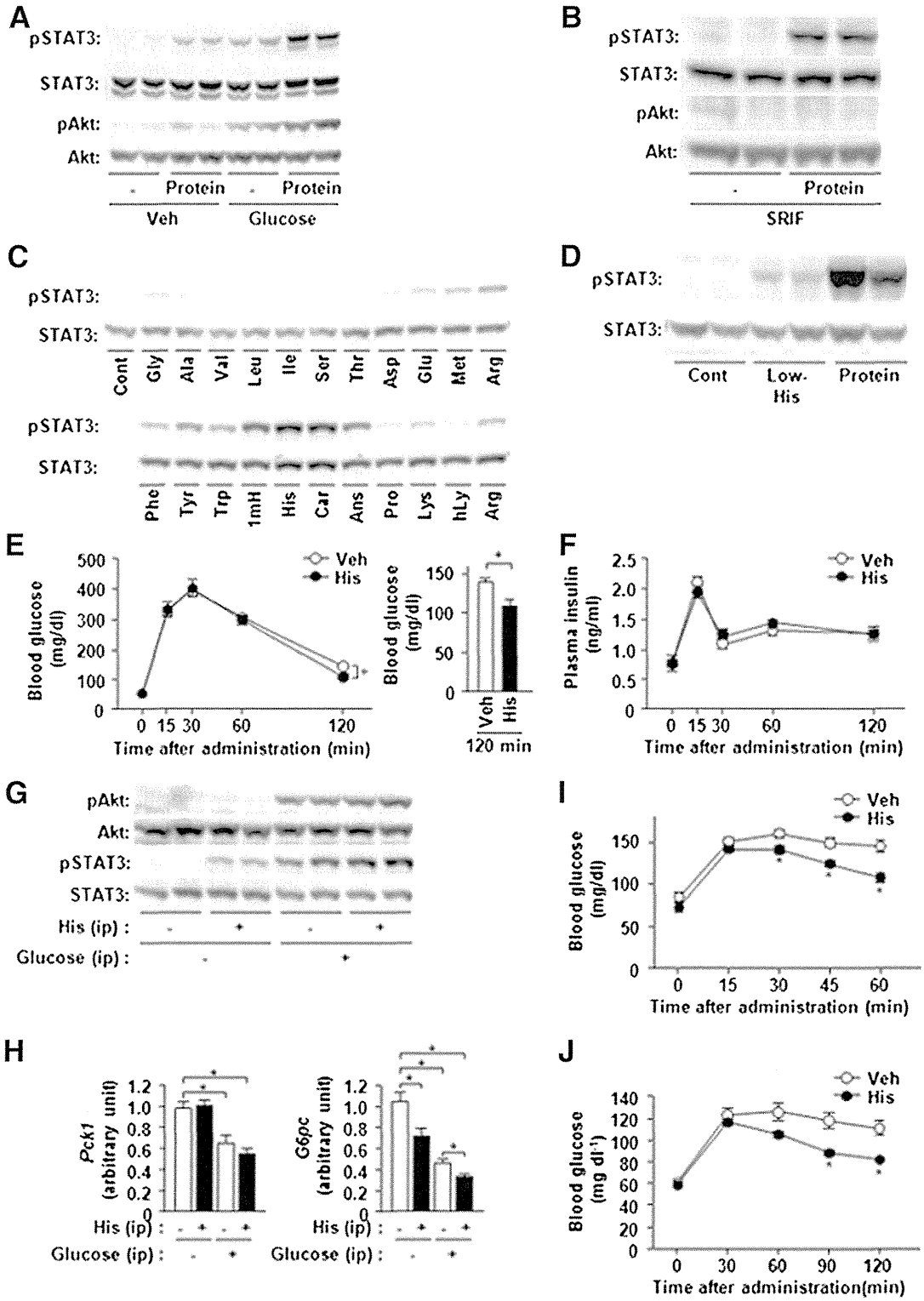

FIG. 1. Phosphorylation of hepatic STAT3 after protein or histidine administration. *A*: Western blotting was performed to analyze the phosphorylation of STAT3 and Akt in the liver at 120 min after the oral administration of protein extract (2 g/kg body wt) and injection of glucose (2 g/kg body wt i.p.) or saline. *B*: Somatostatin was injected continuously at 3 $\mu g \cdot kg^{-1} \cdot min^{-1}$ via the jugular vein, and phosphorylation of hepatic STAT3 and Akt was analyzed at 120 min after the oral administration of protein. *C*: Phosphorylation of hepatic STAT3 was analyzed by Western blotting at 120 min after the intraperitoneal administration of amino acids (0.5 mmol/kg). The experiment was performed in quadruplicate ($n = 4$), and samples were combined for Western blot analysis. 1 mH, 1-methyl-histidine; Ans, anserine; Car, carnosine; and hLy, hydroxylysine. *D*: Phosphorylation of STAT3 was analyzed at 120 min after the oral administration of protein or Low-His. *E* and *F*: A glucose tolerance test was performed with the intraperitoneal administration of histidine (His) or saline (Veh). Changes in blood glucose levels (*E*) (*left panel*), blood glucose levels at 120 min after glucose loading (*E*) (*right panel*), and changes in plasma insulin levels (*F*) are shown. $^*P < 0.05$ ($n = 10$). *G* and *H*: Western blotting analysis of hepatic STAT3 and Akt phosphorylation (*G*) and quantitative PCR analysis of *Pck1* and *G6pc* gene expression (*H*) were performed at 120 min after the intraperitoneal injection of histidine or saline (-) and glucose (2 g/kg body wt). $^*P < 0.05$ ($n = 5$). *I* and *J*: A fructose (*I*) and pyruvate (*J*) tolerance test was performed after the intraperitoneal administration of histidine or saline. $^*P < 0.05$ ($n = 10$). Cont, control.